Modeling hydropower operations at the scale of a power grid: a demand-based approach

Laure Baratgin[1,2], Jan Polcher[1], Patrice Dumas[3], and Philippe Quirion[2]

[1]LMD/IPSL, École Polytechnique, Institut Polytechnique de Paris, ENS, PSL Research University, Sorbonne Université, CNRS, Palaiseau France
[2]CIRED, AgroParisTech, CNRS, Ecole des Ponts Paris Tech, CIRAD, EHESS, Nogent sur Marne Cedex, France
[3]CIRAD, UMR CIRED, F-34398 Montpellier, France

Correspondence: Laure Baratgin (laure.baratgin@lmd.ipsl.fr)

Abstract. Climate change and evolving water management practices may have a profound impact on hydropower generation. While hydrological models have been widely used to assess these effects, they often present some limitations. A major challenge lies in the modeling of release decisions for hydropower reservoirs, which result from intricate trade-offs, involving power sector dispatch, competing water uses, and the spatial allocation of power generation within the grid.

To address this gap, this study introduces a novel demand-based approach for integrating hydropower within the routing module of land surface models. First, hydropower infrastructures are placed in coherence with the hydrological network and links are built between hydropower plants and their supplying reservoirs to explicitly represent water transfers built for hydropower generation. Then, coordinated dam operation is simulated by distributing a prescribed electric demand to be satisfied by hydropower over the different power plants on the power grid, while considering the operational constraints associated with the multipurpose nature of most dams.

To validate our approach, this framework is implemented within the water transport scheme of a land surface model and assessed with the case study of the French electrical system. We drive the model with a high-resolution atmospheric reanalysis and prescribe the observed national hydropower production as the total power demand to be met by hydropower infrastructures. By comparing the simulated evolution of the stock in reservoirs to the observations, we find that the model simulates realistic operations of reservoirs and successfully satisfies hydropower production demands over the entire period. We highlight the roles of uncertainties in estimated precipitation and of the limited knowledge of hydropower infrastructure on the estimation of production. Finally, we show that such an integration of hydropower operations in the model improves the simulations of river discharges in mountainous catchments affected by hydropower.

1 Introduction

1.1 Background and motivation

Hydroelectric power is set to play a pivotal role in numerous power grids in the coming decades, offering low-carbon and dispatchable generation capacity. However, power grids that rely on hydropower production are subject to the unpredictability of weather and climate. Consequently, assessing the potential impact of drought events or climate change on hydropower production is a major concern for the development of resilient energy systems.

Numerous studies (Lehner et al., 2005; Van Vliet et al., 2016; Turner et al., 2017; Zhou et al., 2018; Voisin et al., 2020) have revealed the significant impact of climate change on hydropower production in certain regions, including southwestern Europe and France. These studies typically employ global hydrological models (GHMs) or land surface models (LSMs) driven by atmospheric projections generated by global climate models (GCMs) (Turner and Voisin, 2022). These models simulate the regional-scale hydrological cycle, offering gridded assessments of surface runoff and streamflow, which are then used to derive hydropower production estimates.

However, the estimation process from streamflow to hydropower production is challenging for three reasons. Firstly, water can be stored in reservoirs for future use. The timing of reservoir releases is then the result of the management of the power grid and the coordinated operation of other plants across various water catchments. Representing these intricate economic and spatial trade-offs, which drive the operation of hydroelectric reservoirs, in climate models is complex. Secondly, reservoirs that feed hydropower plants are often multi-purpose and operated to satisfy other water uses, namely irrigation or tourism. Thirdly, hydropower production can involve inter-catchment water transfers, particularly prevalent in mountainous regions where water is stored at higher elevations before being channeled to power plants located in the valleys. Representing these short-scale processes within regional models poses further complications.

Existing studies adopt diverse strategies to represent these complex operations of hydroelectric reservoirs, which are generally categorized into two main approaches (Nazemi and Wheater, 2015b). On the one hand, simulation algorithms rely on predefined rules to compute reservoir releases. These rules are often a function of reservoir inflow and filling level inspired by the pioneering work of Hanasaki et al. (2006) (e.g. in MOSART-WM a reservoir scheme used by Zhou et al. (2018); Voisin et al. (2020); Ralston Fonseca et al. (2021)) or defined based on target curves of water levels from which the release is determined (e.g. in VIC-RES (Dang et al., 2020) used by Chowdhury et al. (2021); Siala et al. (2021)). Such a method accounts for the seasonal behavior of hydroelectric reservoirs, but it misses the representation of short-term operations, as no links with the power system needs are made. On the other hand, optimization algorithms based on the pioneering work of Haddeland et al. (2006) determine the optimal release for each dam. The objective function to optimize varies depending on the reservoir's primary purpose, aiming to maximize individual production for hydroelectric reservoirs. However, these methods consider each reservoir independently and often employ large time steps (monthly) to reduce computational strain.

When the models differentiate the various uses of reservoirs, they categorize the reservoirs based solely on their primary purpose (Abeshu et al., 2023). This approach does not allow for the representation of all the constraints that apply to most hydroelectric reservoirs, which are often multi-purpose. Moreover, none of these studies operate the dams as a network that takes advantage of the spatial complementarity of climatic regions or cascading effects.

Finally, none of these large-scale studies explicitly model the water transfers from reservoirs to power plants. In most cases, the flow rate within the grid cell where the power plant is located is used to estimate its production, without considering the actual location of the reservoir (Van Vliet et al., 2016; Zhou et al., 2018; Voisin et al., 2020). However, this approach may lead to an overestimation of production, as the flow rate at the plant site is greater than at an upstream dam site, and inter-basin transfers may also occur.

1.2 Objectives

The objective of this study is to present the original methodology we developed to estimate hydropower production at the scale of a regional power grid. This methodology is based on the simulations of a GHM or LSM and addresses the three challenges previously identified: (i) considering the coordinated management of the entire power system at the scale of the power grid; (ii) accounting for the multi-purposes objective of reservoirs that store water for hydropower production; (iii) representing the inter-catchment water transfers from reservoirs to power plants.

Our approach is inspired by the demand-based algorithms used for irrigation reservoir management, pioneered by Hanasaki et al. (2006). In these algorithms, a demand point (irrigated area) is connected to a supply point (river), with the water demand of the downstream irrigated area driving upstream reservoir releases (Nazemi and Wheater, 2015b; Zhou et al., 2021).

In our methodology, hydropower plants are linked to reservoirs whose releases depend on the demand for hydropower production. At the geographical scale of the whole power grid, the balance between electricity demand and generation is the primary concern, regardless of the specific locations of consumption and generation. Consequently, we assume that all hydroelectric reservoirs in the power grid may contribute to satisfying the demand for dispatchable hydropower production defined at the grid level, as a result of the power system dispatch decisions. Power dispatching involves deciding which types of power plants are activated to satisfy the total power demand, based on the cost and availability of generation resources. We do not explicitly represent this side of the power system decisions but consider a corresponding demand for dispatchable hydropower to drive the operation of the hydroelectric reservoirs in our model.

We implement the proposed methodology in the ORCHIDEE LSM (Krinner et al., 2005), but it aims to be usable in any LSM or GHM. The first steps of building a river network that represents inter-catchment hydropower transfers and defining rules for reservoir releases are generic and only require basic information on dam and plant characteristics. To validate the effectiveness of the approach, we apply it to the French power grid. A calibration step is added, which requires more information on individual plants to adjust the efficiencies of the power plants. Finally, simulated and actual operations of hydroelectric reservoirs are compared.

The paper is structured as follows: Sect. 2 describes the proposed methodology and its originality. Sect. 3 introduces the data and methods used for our case study of the French power grid and assesses the performance of ORCHIDEE in reproducing river discharges over this area. Sect. 4 details the modeling results, and finally Sect. 5 discusses these results and concludes by outlining future perspectives of research.

2 Model

Our method relies on three main novelties: building a river network that includes most hydropower-related infrastructures and represents inter-basin hydropower transfers (Sect. 2.1), implementing a reservoir scheme that accounts for multi-purpose reservoirs (Sect. 2.2), and using hydropower demand to infer hydroelectric reservoir operations (Sect. 2.3).

2.1 Definition of a routing network that includes hydropower connections

The spatial resolution of GHMs or LSMs is typically constrained by the atmospheric grid of the forcing files, which is generally set at 0.5° (approximately 50 km) for large-scale implementations and 0.1° (approximately 10 km) for regional implementations. However, human activities such as irrigation or urban areas operate at much higher spatial resolutions, typically within a few kilometers. The concept of hydrological transfer units (HTUs) has been introduced in routing modules to bridge the gap between the differing resolutions of atmospheric and hydrological processes resolutions and to provide the opportunity to incorporate human activities in such models (Nguyen-Quang et al., 2018). HTUs correspond to sub-grid river basins, which permit runoff generated in one atmospheric grid cell to flow into multiple neighboring atmospheric grid cells. The introduction of these smaller units allows for a more accurate representation of the river system and its interaction with human activities, including hydropower.

Three types of hydropower plants are distinguished, with different implications on locations:

– **Run-of-river plants** lack any storage capacity and generate electricity according to the instantaneous river discharge at the plant location. There is no difficulty involved in the location of the plants;

– **Reservoir plants** are fed by reservoirs that can store a specified water volume and are often also used for other purposes, which may constrain the operations of the plant. Electricity production does not necessarily take place at the location of water storage, therefore the plant and the reservoir need to be located separately.;

– **Poundage plants** are defined in some regions as a subcategory of reservoir plants whose upstream reservoir is relatively small and only allows to store water for a short period.

As an example of different locations of reservoir and power plant, the "La Bathie" power plant, the largest reservoir power plant in France, draws water from the Roselend reservoir, which is located about 20 km away (see D). At a kilometric resolution, this implies horizontal water transfers between these two locations (water withdrawal and restitution), which requires the reconstruction of the hydroelectric water supply network within the routing network of ORCHIDEE.

We proceed in three steps as illustrated in Fig. 1. First (Fig. 1-b), we place dams and hydropower plants on a high-resolution river network (MERIT (Yamazaki et al., 2019) is used in this study), based on geo-referenced data and upstream area provided in infrastructure databases. The location procedure is detailed in Appendix A and the infrastructure datasets used for our study of France are presented in Appendix B. Then, we build the adduction network by identifying supposed connections between power plants and dams that feed them (see Appendix A for more details on the procedure to build the adduction network). Finally (Fig. 1-c), we form HTUs by aggregating MERIT pixels in an atmospheric grid cell with the same general flow direction following the procedures described in Nguyen-Quang et al. (2018) and Polcher et al. (2023).

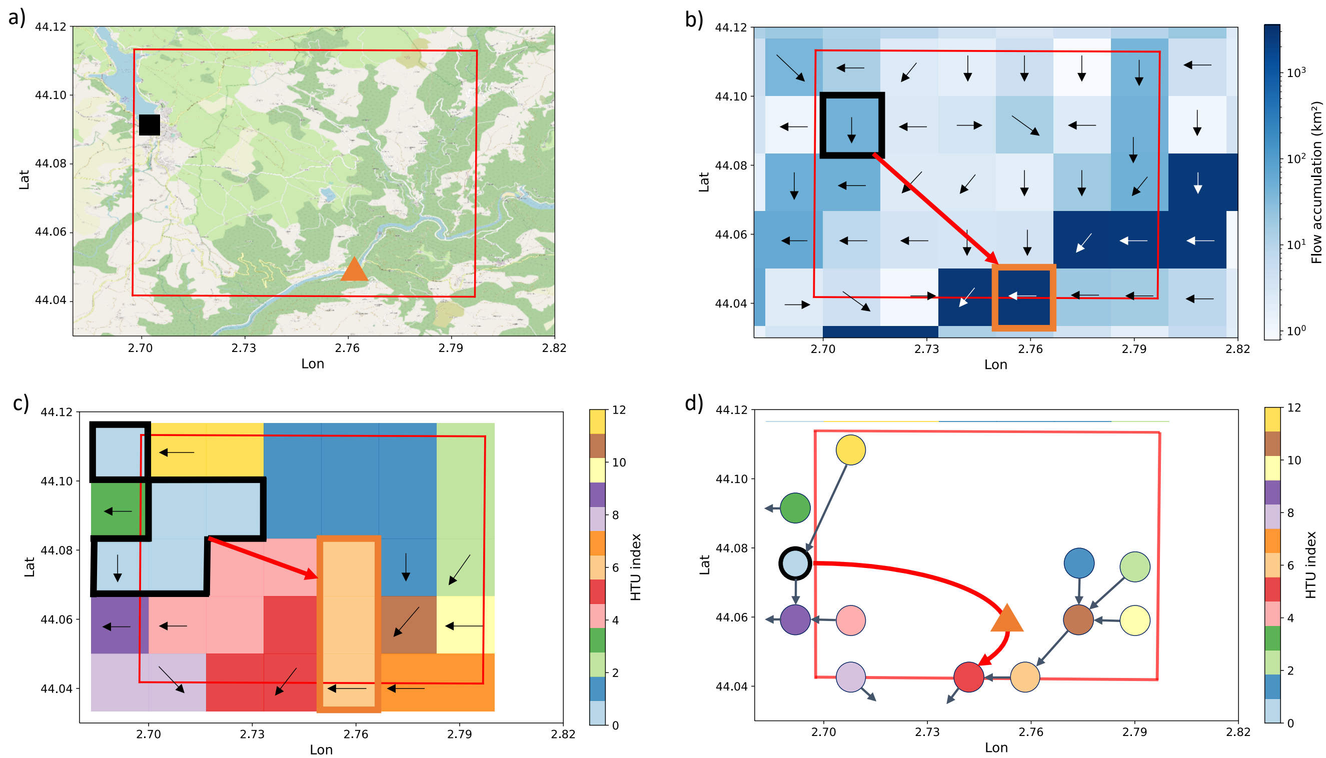

Figure 1. Illustration of the procedure to build ORCHIDEE routing network with the example of Pouget hydropower plant in France. (a) Geographic context of Pouget power plant (orange triangle) and its feeding reservoir (black square indicating the location of the dam). The red grid indicates the atmospheric grid. (b) Flow directions and accumulation for the MERIT pixels overlapping the atmospheric grid. MERIT pixels in which we located the power plant and the dam are respectively indicated in orange and black while the red arrows represent the adduction network link we identify. (c) Resulting HTUs decomposition. The location of the infrastructures is reported in the corresponding HTUs (d) Corresponding HTUs graph. The HTU containing the dam is indicated with a bold black outline while the power plant (orange triangle) is placed on the edge between the reservoir and the HTU downstream from the one in which it has been located.

This procedure results in an HTU network representing natural and human-made water flows. It can be seen as a directional graph (Fig. 1-d) where vertices correspond to HTUs and edges represent directional water flows (natural and human-made for hydropower purposes). Considering this graph, hydropower plants are placed on the edges connecting the HTU of their withdrawal point and the HTU downstream of the one in which they are located. Fig. 2 introduces the notation that will be used throughout the article to index HTUs and edges in such graphs. It shows that the water used to produce electricity can follow a different path from the natural flow out of the reservoir. This approach allows for the representation of this distinction independently of the atmospheric resolution.

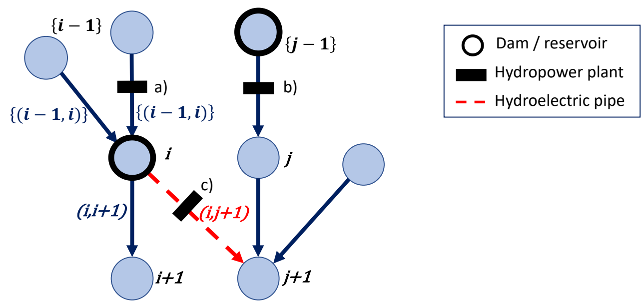

Figure 2. Graph representation of the river routing network built. Each vertex represents an HTU. HTUs containing a dam are represented by bold dark circles. Edges represent existing water flow directions (blue edges for natural water flows and dashed red ones for hydroelectric pipes). Power plants are placed on edges whose water flows they can use to produce power ((a): run-of-river plant, (b)-(c) reservoir or poundage plants)). The indexing convention is also presented on the graph, with integers used for vertices and couples of integers for edges. $i+1$ is the HTU directly downstream of i (natural flow) while $\{i-1\}$ denotes the ensemble of HTU flowing into HTU i. Similarly $(i,i+1)$ is the natural outflow edge from HTU i while $\{(i-1,i)\}$ represent the ensemble of inflow edges into HTU i, including basin transfers.

Attributes and variables describing reservoir and hydropower characteristics of each HTU i and vertex (i,j) are presented in Table 1.

vertex	$V_{tot,i}$	Total maximum storage capacity of the reservoir located in HTU i (m^3)
	$V_{elec,i}, V_{recr,i}, V_{irri,i}$	Maximum storage capacity dedicated to respective water uses (hydropower, recreation, and irrigation) of the reservoir located in HTU i (m^3)
	$H_{dam,i}$	Height of the dam located in HTU i (m)
	$\boldsymbol{V_i(t)}$	**Current total volume in the reservoir located in HTU i (m^3)**
	$V_{min,i}(t)$	Minimal water volume in the reservoir, it evolves with time to account for recreation uses (see Fig. 5) (m^3)
	$h_{res,i}(t)$	Water level in the reservoir (m)
	$A_{res,i}(t)$	Surface of the reservoir (m^2)
edge	$P_{(i,j)}$	Installed hydropower capacity of the plant located on the edge (MW)
	$H_{(i,j)}$	Nominal hydraulic head of the plant located on the edge, obtained with a full reservoir (m)
	$Typ_{(i,j)}$	Hydropower plant type (run-of-river, poundage, or reservoir)
	$\eta_{(i,j)}$	Production efficiency of the plant (conversion of potential energy to power)
	$E_{(i,j)}(t)$	Production of the plant on the edge (MWh)

Table 1. Model attributes and variables describing reservoirs and hydropower. Prognostic variables are distinguished in bold

During calibration (see Sect. 2.5), plants for which the identification of a single reservoir conducts to a significant misrepresentation of the plant's hydropower potential are identified and a correction is made by moving the withdrawal point so that it gathers enough water to ensure the observed production is possible.

2.2 Dams and reservoir parametrization

In the initial version of ORCHIDEE (Polcher et al., 2023), each HTU i contains three natural water stores, characterized by their time constants (slow aquifer, fast aquifer, and stream storage). To represent water management we add a fourth store to the HTUs in which dams have been located to represent water storage in the reservoir (Fig. 3). This section presents the continuity equation for the water volume in this reservoir.

2.2.1 Prognostic equations for water stores

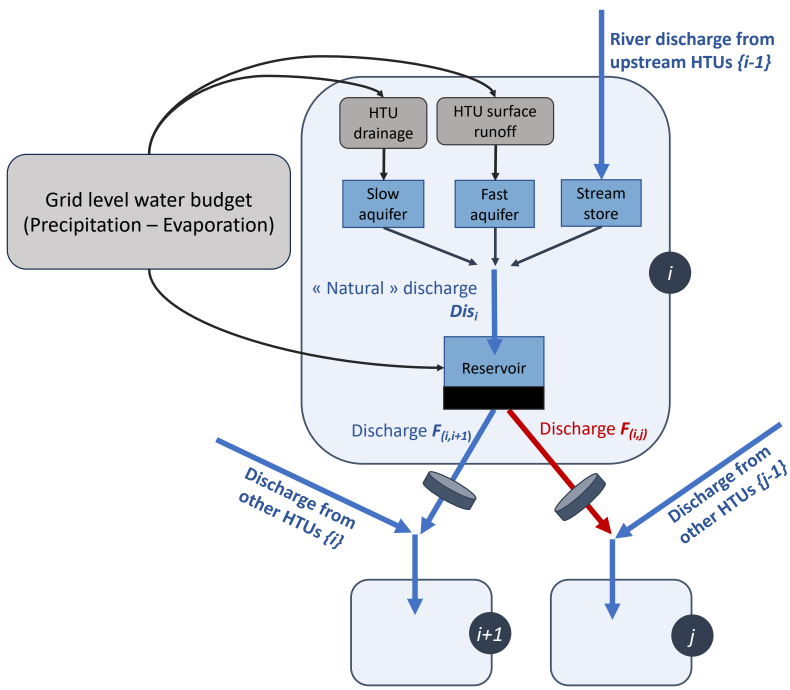

Figure 3. Schematic representation of water stores and flows in an HTU i

As represented in Fig. 3, the fast aquifer is filled by local runoff generated in the HTU, the slow aquifer by local drainage generated in the HTU, and the stream store by the discharge from upstream HTUs. The equations of these natural water stores are detailed in previous publications (Zhou et al., 2021; Polcher et al., 2023). They introduce the respective time constants of the natural stores g_{stream}, g_{fast} and g_{slow} (in unit $h.m^{-1}$) and the topographic index calculated for each HTU τ_i (in unit m^2).

The "natural discharge" $Dis_i(t)$ in the HTU i is generated by summing the outflows of the natural water stores (Eq. (1)). This natural discharge is stored in the reservoir if there is one in the HTU, or routed towards the downstream HTU if there is not.

$$Dis_i(t) = \frac{1}{\tau_i} * \left(\frac{W_{stream,i}(t)}{g_{stream}} + \frac{W_{fast,i}(t)}{g_{fast}} + \frac{W_{slow,i}(t)}{g_{slow}} \right) \quad (1)$$

The prognostic equation on reservoir volume is then given by:

$$\frac{dV_i}{dt}(t) = Dis_i(t) + p_{res,i}(t) - ev_{res,i}(t) - \sum_j F_{(i,j)}(t) \tag{2}$$

where $p_{res,i}(t)$ and $ev_{res,i}(t)$ are respectively direct precipitation and evaporation over the reservoir, and $F_{i,j}(t)$ is the water released from the HTU i to the HTU j, which breakdowns as:

$$F_{(i,j)}(t) = \max\left(F^{ecol}_{(i,j)}(t), F^{irri}_{(i,j)}(t), F^{elec}_{(i,j)}(t)\right) + F^{spill}_{(i,j)}(t) \tag{3}$$

Reservoir releases aim at satisfying the different water demands addressed to the reservoir, which are described in Sect. 2.3. Ecological and irrigation releases are limited by the demands addressed to the reservoir and the water available in the reservoir:

$$F^{ecol}_{(i,j)}(t) = \min\left(D^{ecol}_{(j,i)}(t), \frac{V^{\star}_i(t) - V_{min,i}(t)}{\tau_{res}}\right) \tag{4}$$

$$F^{irri}_{(i,j)}(t) = \min\left(D^{irri}_{(j,i)}(t), \frac{V^{\star}_i(t) - V_{min,i}(t)}{\tau_{res}}\right) \tag{5}$$

where $V^{\star}_i(t)$ is the theoretical volume to be obtained without any release (Eq. (6)) and τ_{res} is the time constant of the reservoir, which we assume to be of the order of magnitude of a few minutes.

$$\frac{dV^{\star}_i}{dt}(t) = Dis_i(t) + p_{res,i}(t) - ev_{res,i}(t) \tag{6}$$

The water released for electricity generation is determined by the production of the plant, computed based on the distribution of the prescribed national demand (see Sect. 2.3).

$$F^{elec}_{(i,j)}(t) = \frac{E_{(i,j)}(t)}{\rho g \eta_{(i,j)} h_{(i,j)}(t)} \tag{7}$$

where ρ is the water density, g is the gravitational constant, $\eta_{(i,j)}$ is the efficiency of the plant (set at 0.9 by default), and $h_{(i,j)}(t)$ is the current hydraulic head, which varies with the water level of the reservoir (Eq. (8)).

$$h_{(i,j)}(t) = H_{(i,j)} - (H_{dam,i} - H_{res,i}(t)) \tag{8}$$

Finally, the spillage is defined as the water overflowing without being used for the different uses.

$$F^{spill}_{(i,j)}(t) = \begin{cases} \max\left(\frac{V^{\star}_i(t) - V_{tot,i}}{\tau_{res}} - \sum_k \max\left(F^{ecol}_{(i,k)}(t), F^{irri}_{(i,k)}(t), F^{elec}_{(i,k)}(t)\right),\ 0\right) & \text{,if } j = i+1 \\ 0 & \text{,else} \end{cases} \tag{9}$$

Ecological and irrigation flows $F^{ecol}_{(i,j)}(t)$ and $F^{irri}_{(i,j)}(t)$ are computed before the other flows, consistently with water management policy in most of the countries.

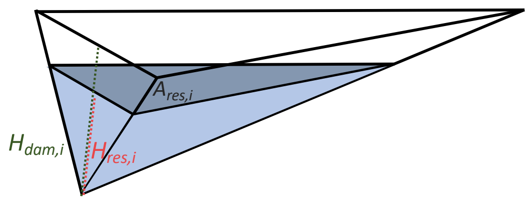

Figure 4. Geometry of the reservoir

2.2.2 Diagnostic variables

As in previous studies (Fekete et al., 2010; Zhou et al., 2018), we represent each reservoir i in the form of a tetrahedron of height $H_{dam,i}$ and volume $V_{tot,i}$ (Fig. 4).

Hence, the relations between the volume $V_i(t)$, the water level $H_{res,i}(t)$ and the area of the reservoir $A_{res,i}(t)$ are given by:

$$H_{res,i}(t) = H_{dam,i} * \left(\frac{V_i(t)}{V_{tot,i}}\right)^{\frac{1}{3}} \tag{10}$$

$$A_{res,i}(t) = \frac{3 * V_i(t)}{H_{res,i}(t)} \tag{11}$$

Direct precipitation and evaporation (m^3/s) over the reservoir are then given by $p_{res,i}(t) = P_i(t) * A_{res,i}(t)$ and $ev_{res,i}(t) = Ev_i(t) * A_{res,i}(t)$ where $P_i(t)$ and $Ev_i(t)$ are respectively the precipitation and evaporation over the HTU i (in m/s).

2.3 Water demands

Reservoirs are designed to store water for a variety of purposes, including energy production, irrigation, tourism, and domestic and industrial uses. As this study focuses on hydroelectric reservoirs, we adopt a simplistic representation of the other water uses and only consider those that can constrain hydropower operations: ecological flows, irrigation, and tourism.

2.3.1 Non-energy demands

In many countries, the environmental laws require a minimum flow $F_{min,(i,i+1)}$ in the watercourse downstream of a dam in i, to guarantee the ecological quality of the river. These minimal flow requirements depend on the region. Details for the French study case are presented in Sect. 3.3.1. Such an ecological demand $D^{ecol}_{(j,i)}(t)$ applies to all reservoirs regardless of their intended use:

$$D^{ecol}_{(j,i)}(t) = \begin{cases} F_{min,(i,i+1)}, & \text{if } j = i+1 \\ 0, & \text{else} \end{cases} \tag{12}$$

Some reservoirs store water for agriculture. Water withdrawals for irrigation can be made either directly from the reservoir or from the downstream river. Withdrawals from the river require a corresponding release from upstream reservoirs to maintain low flows. In this study, the water requirements for irrigation are represented in a highly simplified manner by assuming a need proportional to $F_{min,(i,i+1)}$ during the summer period. $D^{irri}_{(j,i)}(t)$ is then expressed in Eq. (13). The choice of the proportional factor α_{irri} and the delimitation of the summer period may vary across regions. Details for our French case study are presented in Sect. 3.3.1.

$$D^{irri}_{(j,i)}(t) = \begin{cases} \alpha_{irri} * F_{min,(i,i+1)}, & \text{if } j = i+1 \text{ and } V_{irri,i} > 0 \text{ and } t \in Summer \\ 0, & \text{else} \end{cases} \tag{13}$$

Finally, during the summer months, some reservoirs may also become tourist attractions where recreational activities are carried out and require the reservoir to be kept at a high level. To ensure proper reservoir filling during the summer season, dam operators follow a filling guide curve. We define corresponding constraints on $V_{min,i}(t)$ based on previous work and data available for French reservoirs (e.g. François (2013) on the Serre Ponçon reservoir), as shown Fig. 5. By default, the minimum volume is set at 10% of the total capacity of the reservoir and is increased to 90% during the tourist season for the reservoirs concerned.

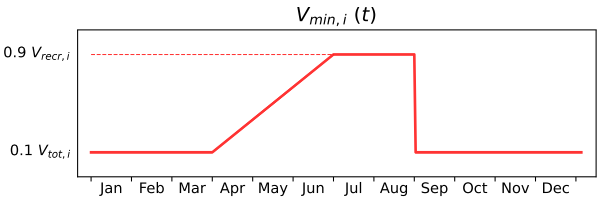

Figure 5. Evolution of the minimum volume constraints during the year

2.3.2 Hydroelectric demand

Production of hydropower plants is the result of the dispatch of the total power demand among the different power plants on the power grid (Stoft, 2002; Wood et al., 2013). Power generation units are called upon from least to most expensive to meet power demand at minimal cost. Run-of-river power plants, whose production is free and non-dispatchable, are called upon first, along with solar and wind power plants, to produce to their maximum potential (as long as it does not exceed total demand, otherwise there is a curtailment of their production). On the contrary, the call upon dispatchable power plants is the result of a much more complex trade-off, aiming to minimize the total power system cost. From the point of view of a social planner, in charge of dispatch decisions and aware of the potentials and costs of all the units available in the network area, as well as the electricity demand, it is thus possible to define at each time step a demand for dispatchable hydroelectric power generation $D_{res}(t)$. This demand (or production target) is defined for the whole grid and needs then to be distributed among the different plants to decide the amount of energy generated $E_{(i,j)}(t)$ at each plant location, that will then drive reservoir release decisions. Indeed, knowing $E_{(i,j)}(t)$, the model deduces the additional water release needed for the plant production (Eq. (7)) and can finally compute the reservoir release based on Eq. (3).

To distribute national demand into individual plants production $E_{(i,j)}(t)$, the model proceeds in two steps.

1) Fatal production: The model starts by going through all the hydropower plants and calculates the energy they can produce or store without additional release, thanks to other releases (ecological or irrigation) or the water expected to overflow.

Associated production $E_{fatal,(i,j)}(t)$ and $E_{spill,(i,j)}(t)$ are computed based on Eq. (14) and (15).

$$E_{fatal,(i,j)}(t) = \min\left(P_{(i,j)}\frac{h_{(i,j)}(t)}{H_{(i,j)}},\ \max\left(F_{ecol,(i,j)}(t), F_{irri,(i,j)}(t)\right) \times \rho g \eta_{(i,j)} h_{(i,j)}(t)\right) \tag{14}$$

$$E_{spill,(i,j)}(t) = \min\Bigg(P_{(i,j)}\frac{h_{(i,j)}(t)}{H_{(i,j)}} - E_{fatal,(i,j)}(t),$$
$$\max\left(\frac{V_i^\star(t) - V_{tot,i}}{\tau_{res}} - \max\left(F_{ecol,(i,i+1)}(t)\ ,\ F_{irri,(i,i+1)}(t)\right), 0\right) \times \rho g \eta_{(i,j)} h_{(i,j)}(t)\Bigg) \tag{15}$$

The remaining production demand to dispatch is then $D_{res}(t) - \sum_{Typ(i,j)\in\{poundage,reservoir\}}(E_{fatal,(i,j)}(t) + E_{spill,(i,j)}(t))$.

2) Reservoirs withdrawals: If there is any national production demand left to dispatch ($D_{res}(t) > 0$), it should be produced by withdrawing water from the reservoirs. In this study, we consider that the reservoirs are used in the decreasing order of their relative filling to produce power while respecting production constraints (installed capacity of the plant and the remaining volume of water in the reservoir). The remaining production is dispatched following this rule, until either all remaining production demand has been satisfied, or no more plants can produce. This rule leads to the equalization of relative filling at the end of each time step. This is equivalent to implementing a uniform rule curve for all reservoirs, as has been done in Dang et al. (2020). Another advantage of this rule is that it leads to a production spread out over the whole territory. All plants are required to produce a little power each day, close to the so-called stable productions modeled in other studies (Sterl et al., 2020).

2.4 Validation diagnostics

The performance of our model to estimate hydropower production will be assessed based on three main diagnostics: the annual hydropower potential (AHP) simulated at each individual plant, the hydraulic stock simulated at the national level, and the time series of simulated production by hydropower plant type.

We define $AHP_{(i,j)}(y)$ as the maximum energy that could be produced by the plant (i,j) over the year y in our simulation. To compute it, we run a simulation in which the demand for dispatchable hydropower $D_{res,t}$ is fixed to infinite, leading all hydroelectric reservoirs to release water within the limits of water availability and the installed capacity of the plant. The simulated water flow $F_{i,j}(t)$ at the plant location is then used to compute $AHP_{(i,j)}(y)$ based on Eq. (16), considering the average head of each plant $\overline{h_{(i,j)}}$, which is determined based on Eq. (8), taking the average reservoir water level.

$$AHP_{(i,j)}(y) = \int_{t\ in\ y} \min\left(\rho g \eta_{(i,j)} \overline{h_{(i,j)}} F_{(i,j)}(t)\ ,\ P_{(i,j)}\right) dt \tag{16}$$

The hydraulic stock is the total energy that can be produced using energy stored in all the reservoirs of reservoir plants belonging to the power grid, it is defined by (Eq. (17)).

$$S(t) = \sum_{(i,j) s.a. Typ_{(i,j)} = reservoir} \int_{V_{min,i}(t)}^{V_i(t)} \rho g \eta_{(i,j)} h_{(i,j)}(V)\, dV \tag{17}$$

Finally, for a hydropower plant type k (run-of-river or reservoir), the simulated production $E_k(t)$ is given by:

$$E_k(t) = \sum_{(i,j) s.a. Typ_{(i,j)}=k} E_{(i,j)}(t). \tag{18}$$

2.5 Calibration

A calibration step is performed based on the comparison of simulated AHP and observed production at each individual plant, provided that such data is available. The objective of this step is to identify and correct errors from different sources, which are discussed in this section. The calibration procedure then varies according to the type of power plant.

2.5.1 Run-of-river plants

A discrepancy between the simulated AHP of a run-of-river plant and its historical production can be attributed to five factors:

1. A hydro-meteorological bias may result in discrepancies in river discharges between the model and the actual river conditions;
2. An inexact location of the hydropower plants during the placement on the HTU graph may lead to inaccurate estimations of the available discharge at the plant location;
3. We assume that the plant can harness the entire river volume. In reality, the river can be divided into several branches, with only one of them passing through the plant;
4. Plants efficiencies are assumed to be equal for all plants and constant to 0.9. In reality, the efficiency of a hydropower plant depends on the type of hydroelectric turbine that is used (the choice is made based on the plant's rated head and flow) and varies with the flow rate;
5. We assume that plants produce at their maximum potential. However, in reality, a plant may be unavailable for a period of time due to maintenance. Moreover, some of the plant's potential can be reserved for ancillary services to the grid or curtailed if the non-dispatchable potential production of renewables exceeds the power demand. This can reduce the actual production compared to the potential.

As in previous studies (Wagner et al., 2017; Zhou et al., 2018), the unknown efficiency of the power plant $\eta_{(i,j)}$ is adjusted to calibrate the model to the historical annual generation data based on previously estimated bias (Eq. (19)). Such calibration corrects the total error without differentiating its source.

$$\eta_{(i,j)} = \frac{1}{0.9} * \overline{\frac{E_{(i,j)}(y)}{AHP_{(i,j)}(y)}} \tag{19}$$

2.5.2 Poundage and reservoir power plants

Over a year, all the water entering the reservoir i of a plant (i,j) could either contribute to the annual production of the plant $E_{(i,j)}(y)$, to the annual change of the hydraulic stock in the reservoir $\Delta S_i(y)$ or spill without generating power.

As for run-of-river plants, differences in simulated AHP and observed production can have different sources. In addition to the five errors listed above, a sixth possible error, related to the adduction network, should also be considered. Indeed, we assume in our model that each plant is only fed by one reservoir, which can lead to an underestimation of the plant production if some other water inputs are non-negligible. To account for these different error sources, we calibrate the model in two successive steps:

- Step 1: Dams with a large negative bias (inferior to -50 %) are shifted downstream from their original location to take into account the computed deviation. This can be interpreted as the addition of water inlets for the power plant based on the topography such that the power plant receives enough water. Most concerned areas are located in mountains, where the water intakes are quite close geographically (on the same atmospheric grid) and therefore subject to the same precipitation, which allows us to assume that the water available per unit of area is similar.

- Step 2: Once the network error is corrected, the efficiencies of the plants are adjusted to match the observed production, as with run-of-river (Eq. (19)).

3 Data and methods for the test case over France

3.1 ORCHIDEE setup

In this study, ORCHIDEE is run in stand-alone mode, forced with the SAFRAN meteorological data set (Quintana-Segui et al., 2008). SAFRAN (Système d'Analyse Fournissant des Renseignements Atmosphériques à la Neige) is a surface reanalysis resulting from the optimal interpolation between the vertical profiles of the atmosphere derived from ERA-40 atmospheric reanalysis and surface observations. It provides the required atmospheric variables - temperature, relative humidity at two meters, wind speed, downward radiation (shortwaves and longwaves), and precipitation (solid and liquid) - at an hourly time step over an 8×8 km grid that covers France and upstream part of its catchments beyond its borders.

To estimate the sensitivity of ORCHIDEE's simulations to the uncertainties of precipitation, we built two alternative atmospheric forcings by replacing precipitation data in SAFRAN with other precipitation datasets: COMEPHORE (Tabary et al., 2012) and SPAZM (Gottardi et al., 2008). These datasets are presented in detail in Appendix C1 and their relative differences with SAFRAN are displayed in Fig. C1.

COMEPHORE dataset provides observations of surface precipitation accumulation over metropolitan France at an hourly and kilometric resolution based on a synthesis of radar and rain gauge data. We build a meteorologic dataset SAF_COM by replacing precipitation data in SAFRAN with data from COMEPHORE. As COMEPHORE does not distinguish solid and liquid precipitations, we keep SAFRAN's hourly ratio of solid/liquid precipitations when possible and discriminate based on the air temperature otherwise. The differences in annual mean precipitation between SAFRAN and COMEPHORE are generally small, with an average deviation inferior to 1.0% in COMEPHORE compared to SAFRAN (Fig. C1). However, we find a small seasonal bias as this average deviation goes from -2.0% for the Winter period to +1.9% in the Summer. Moreover, discrepancies increase dramatically in mountainous regions, especially in the Alps and in the Pyrenees. For grid points with an average elevation above 1000m, the annual mean precipitation in COMEPHORE is, on average, 10.4% lower.

SPAZM is a daily reanalysis of precipitation at the kilometer scale, developed by EDF, the main electricity producer in France. We interpolate the daily precipitation data from SPAZM to the hourly scale and merge it with SAFRAN data to create the alternative forcing dataset SAF_SPAZM. As for SAF_COM, we keep SAFRAN's hourly ratio of solid/liquid precipitations when possible. Compared to SAFRAN, precipitations are on average 2.7% higher in SPAZM with an average bias of 7.0% in Summer, against 2.1% in Winter. Bias is heterogeneously spread over France (Fig. C1) with bigger differences on the highest reliefs, without a clear sign (average deviation of +3.9% for grid points above 1000m).

Appendix E provides an extensive assessment and discussion of hydro-meteorological biases in ORCHIDEE simulations over French rivers. In particular, we identified uncertainties in observed precipitation as a main contributor to the error in simulated discharge, especially in the mountains.

The vegetation distribution map used in ORCHIDEE is derived from the ESA-CCI Land Cover dataset at 0.05° resolution for the year 2010. The soil background albedo map is derived from the MODIS albedo dataset aggregated at 0.5° resolution. Soil texture distribution maps are obtained from Reynolds map (Reynolds et al., 2000) at 5-arc-min resolution with 12 USDA soil texture classes (at 30 cm depth). In this study, ORCHIDEE performs the energy and water budgets at a 15-minute time step and hydropower operations are performed at the same time step. Given that the time step is greater than the time constant of reservoirs, we consider that reservoir spillage always occurs within a single time step.

3.2 Hydroelectric infrastructure

The infrastructure datasets are presented in detail in Appendix B. We use reservoir data from GRanD (Global Reservoirs and Dams) (Lehner et al., 2011) and CFBR (CFBR, 2021) datasets. Data provided in these datasets allow us to validate the assumption about reservoir geometry (Fig. 4). For hydropower plants, we use data from the EU Joint Research Center hydropower plants database (European Commission and Joint Research Centre (JRC), 2019) and national registers of electricity generation and storage facilities published annually by the French TSO (ODRÉ, 2016, 2018).

Following the procedure outlined in Fig. 1, we locate the infrastructures on the MERIT river network and construct the HTUs routing graph based on the simplification of this MERIT network (resolution of 2km) on the SAFRAN atmospheric grid (resolution of 8 km). HTUs area can thus theoretically vary from 0 to 64 km^2 and the average area of HTUs in our graph is 4.73 km^2. The upstream area of an HTU is defined recursively as the sum of the HTU area and the upstream area of all its tributaries. For each hydroelectric infrastructure, we compare in Fig. 6 its reference upstream area (from the database or MERIT network) to the upstream area of the HTU in which it is located. For most of the structures, the positioning error is lower than 20%. Some dams with a small upstream area are, however, located in HTUs with a higher upstream area, due to resolution constraints.

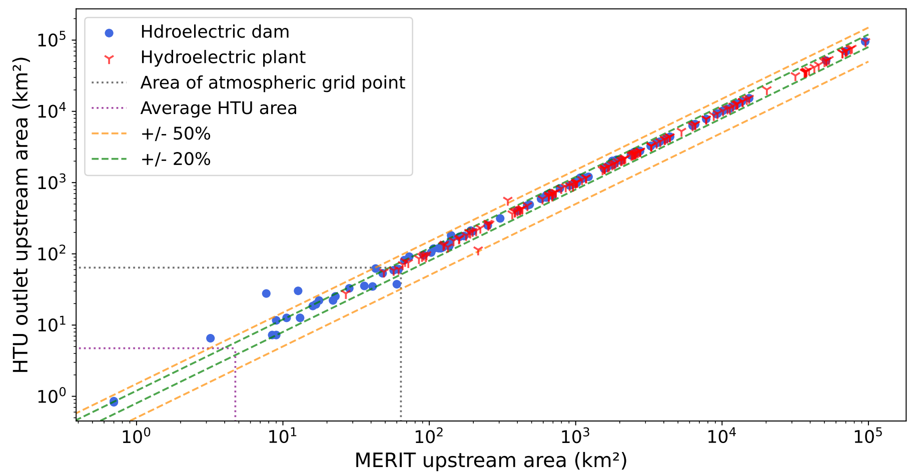

Figure 6. Comparison of the initial upstream area of the infrastructure (referenced in the database or upstream area of the MERIT pixel on which it is placed) with its final upstream area in the HTUs graph. Blue dots represent hydroelectric reservoirs (reservoirs that have been associated with power plants during the adduction network building step) and red signs represent hydropower plants. Green and orange dashed lines delineate a respective error of +/- 20% and +/- 50% while grey and purple dotted lines refer to the respective atmospheric grid point area and average area of an HTU.

3.3 Data for water demands and validation

3.3.1 Ecological and irrigation demands

In France, minimal flow requirements are defined relatively to the mean interannual flow upstream of the dam $\overline{Dis_i}$ (Code de l'Environnement, Article L214-18). They are summarized in Table 2. We ran a twenty-year SAFRAN simulation without reservoir operations to calculate $\overline{Dis_i}$ at dam locations.

	$\overline{Dis_i} > 80m^3/s$	$\overline{Dis_i} < 80m^3/s$
Dam intended for hydropower purpose	$F_{min,(i,i+1)}(t) = 5\% * \overline{Dis_i}$ or flow immediately upstream of the dam if it is lower	$F_{min,(i,i+1)}(t) = 5\% * \overline{Dis_i}$ or flow immediately upstream of the dam if it is lower
Dam intended for other purpose	$F_{min,(i,i+1)}(t) = 5\% * \overline{Dis_i}$ or flow immediately upstream of the dam if it is lower	$F_{min,(i,i+1)}(t) = 10\% * \overline{Dis_i}$ or flow immediately upstream of the dam if it is lower

Table 2. French legal requirements for ecological flow, $\overline{Dis_i}$ is the mean interannual flow downstream of the dam

To account for the irrigation purposes of some reservoirs, we increase the minimal flow requirement downstream of reservoirs intended for irrigation during the summer period (June 1st to September 30th) by setting $\alpha_{irri} = 8$. This choice is based on information available from French reservoir concession contracts, which sometimes specify the volume of water reserved for irrigation. In the case of Serre-Ponçon, for example, the concession contract stipulates a reserve of 200 million m^3, to be used for irrigation, between July 1 and September 30. If we consider a constant withdrawal spanning three months, this corresponds to a $25m^3/s$ flow, which is 45% of the $55m^3/s$ mean interannual flow at this location, and thus 9 times larger than F_{min}, which is set to 5%, as explained above.

3.3.2 Hydropower production demand

As this study aims to validate our proposed reservoir operations model, we take the historical time series of production as the hydropower demand prescribed to the model. We can thus assess if the reservoir operations performed by the model when it is forced by the historical atmospheric dataset can meet the observed production. Data of observed production for hydropower plants in the French power grid are published from 2015 onwards by the French electricity transmission system operator RTE at a 30-minute time step for 2 categories of plants (RTE, a):

- **River production** $D_{river,t}$ that gathers the production of pure run-of-river power plants and poundage power plants (reservoir plants with a storage below 400h)
- **Reservoir production** $D_{res,t}$ that gathers the production of reservoir power plants with a greater storage capacity

In our model, $D_{river,t}$ is then used to drive the production of run-of-river and poundage power plants, while $D_{res,t}$ is used for the reservoir power plants with greater storage capacity, both using the method described in 2.3.2. We use the classification established by RTE and illustrated in Fig. B2.

3.3.3 Validation data

In France, hydroelectricity is produced by companies that do not share precise data on the production of their power plants or the filling of the reservoirs they manage. Similarly, discharge data from gauging stations near hydroelectric power plants are often inaccessible to the public. This limits the available data for validating our model.

However, as a delegate of public services, RTE provides data, often aggregated at the national level, which allows us to calibrate and validate our model as shown in the following two sections.

The available data is:

- National time series of production by hydroelectric sector (river and reservoir) at 30-minute time step from 2015 (RTE, a) - which are the time series used for the hydropower production demand;
- Annual production of each hydroelectric power plant for the years 2015, 2016, and 2018 (ODRÉ, 2015, 2016, 2018);
- Weekly hydraulic stock (Eq. (17)) at national level from 2014 to 2020 (RTE, b);

As mentioned in Appendix B, our final hydropower plants dataset does not include all the hydropower plants installed in France. However, using annual production data of each plant provided by (ODRÉ, 2015, 2016, 2018), we can quantify the share of the national production provided by the power plants in our database. This enables us to compute a factor to convert the actual production of national time series (RTE, a) into representative production in our model both for prescribing the production demand and comparing the results. The calculation of such conversion factors is presented in Table B2.

We also compute the maximal hydraulic stock of the reservoirs associated with the power plants in our database using Eq. (17) and data from our plants and reservoirs databases. We obtain $S_{max} = 3.66$ *TWh*, which is quite close to the 3.59 *TWh* value reported by RTE (RTE, b). Therefore, we can consider that our database covers all the available storage and that missing hydropower capacity is linked to negligible reservoirs.

4 Results

4.1 Calibration

We present here the application of the calibration process to the French study case. We assess the discrepancy between the AHP simulated by the model (Eq. (16)), and the observed annual production at each power plant for the years with available data. The likely origin of these discrepancies is then discussed. Finally, the calibration process is validated by comparing annual potentials simulated in ORCHIDEE to the observed annual production at the national level for an extended period (data available from 2000 to 2020). We choose to use SAFRAN forcing as a reference for the calibration step, as this dataset is widely used in regional studies of France.

4.1.1 Discrepancies between AHP and the historical production

Figure 7 shows the average relative bias in simulated AHP compared to observed production for the three years with available data for the run-of-river plants in our database. For the majority of plants, the bias in hydropower potential is comparable to the bias in river discharge computed at neighboring stations displayed in Fig. E1, indicating that it mainly comes from the hydro-meteorological error (reason 1 of the list presented in Sect.2.5). At the Caderousse and Gambsheim power plants, located in Fig. 7, a stronger positive bias is found. At these locations, only part of the river passes through the plant, which may contribute to the observed bias (reason 3). The calibration leads to obtained efficiencies ranging from 0.43 to 1.31 with a median value of 0.88.

Over a year, all the water entering the reservoir of a reservoir or poundage power plant could either contribute to the annual production of the plant $E_{(i,j)}(y)$, to the annual change of the hydraulic stock in the reservoir $\Delta S_i(y)$ or spill without generating power. Observed production $E_{(i,j)}(y)$ is available for the three years mentioned earlier, however observations of the change of the hydraulic stock are only available at the national level for the national stock $\Delta S_{obs}(y) = \sum_{i \text{ in res}} \Delta S_i(y)$. To compare simulated AHPs with observations of production and stored energy, we make the two following assumptions: (i) spillages that do not produce power can be neglected and (ii) the change in the hydraulic stock is homogeneous across all reservoirs: $\forall i, \Delta S_i(y) = \Delta S_{obs}(y) \times \frac{S_{max}}{S_{i,max}}$. In Fig. 8, we plot the average bias of $AHP_{(i,j)}(y)$ relative to observed net production $E_{(i,j)}(y) + \Delta S_i(y)$ for the three years for which data is available. It enables us to distinguish two types of bias in the simulated AHP, suggesting that two main error sources can be distinguished:

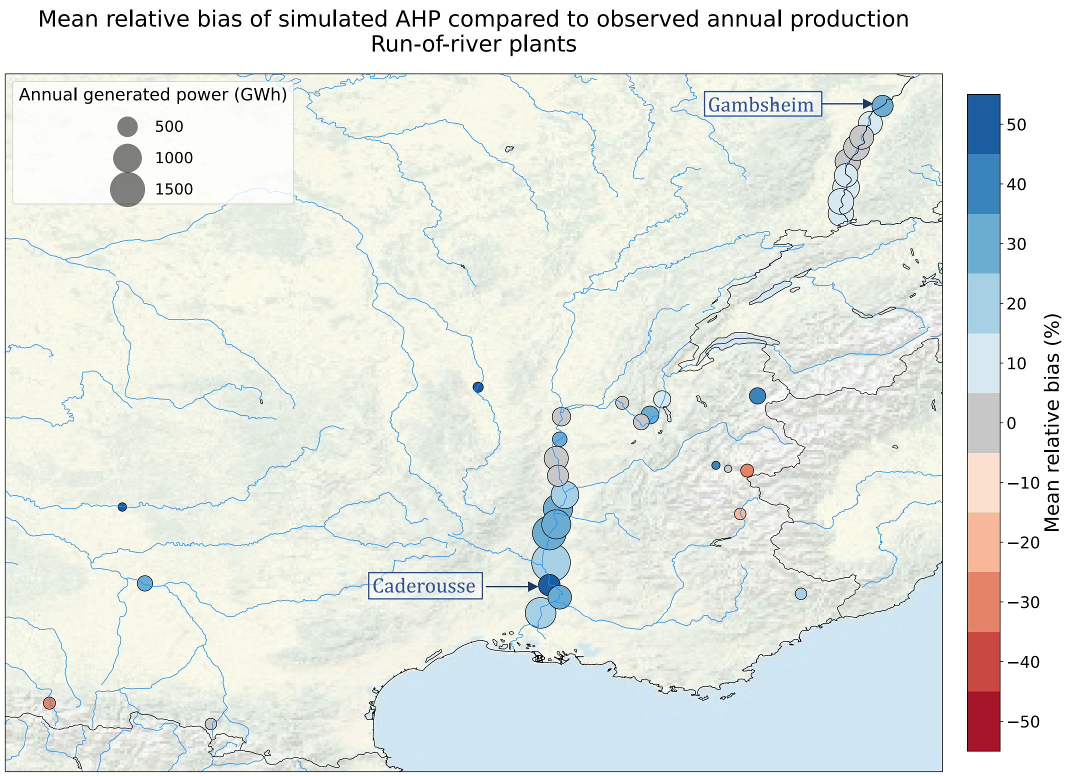

Figure 7. Average relative bias of simulated annual hydropower potential compared to observed historical production for run-of-river plants with available data. The point size corresponds to the average annual production.
Source: authors, based on a layer by U.S. National Park Service

– Plants that have an absolute bias inferior to 50% (represented by circles in Fig. 8). Their biases are generally similar to the one of discharge for neighboring stations in Fig. E1.

– Plants that have a bias inferior to -50% (represented by pentagons in Fig. 8). These plants are mainly located in mountain areas and have a negative bias larger than the one of the discharges in this area. Moreover, their biases have a small interannual variance, indicating that the error is stable in time (not shown).

4.1.2 Validation of the calibration

The performance of the calibrated model is assessed by comparing potentials simulated by the calibrated model forced by SAFRAN with the historical annual production (RTE, a) for the different categories of power plants over the whole period 2010-2020. We assume that hydropower is used as much as possible and that the production is well managed so that the AHP is a good proxy to compare with the actual production. For a given category, the simulated annual potential is computed by summing the AHP of all plants belonging to this category. For poundage and reservoir plants, we directly compare this

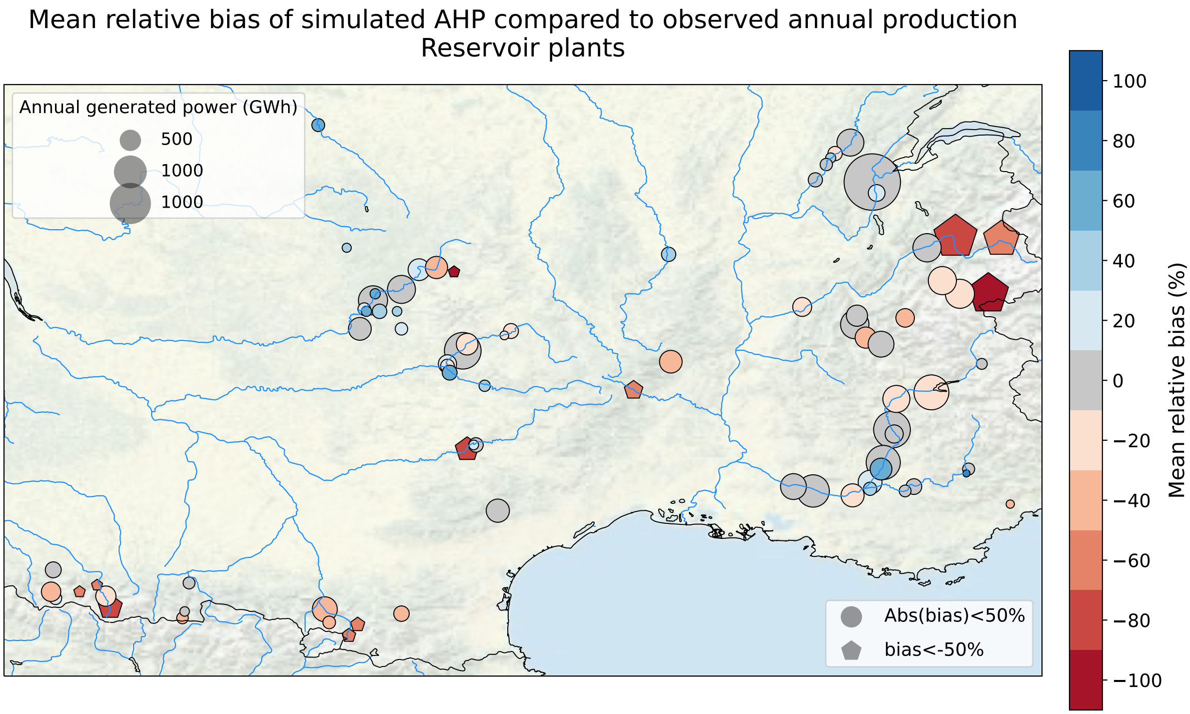

Figure 8. Average bias in the simulated AHP compared to the observed historical net annual production of reservoir and poundage power plants. The point size corresponds to the average annual production of the plant.
Source: authors, based on a layer by U.S. National Park Service

aggregated potential to the historical production, as stock data (RTE, b) is not available for the whole period. This relies on the assumption that the national stock returns to its initial value at the end of each year.

The calibration appears to be robust as a very small bias (less than 3%) is obtained when comparing the simulated potentials to the observed production (Fig. 9). The relative differences in annual production are on average lower than 10%. This indicates that the model is able to capture the overall pattern of interannual variability of the observed production.

We also explore the sensitivity of our model and calibration procedure to the uncertainties in precipitation forcings highlighted in Fig. C1 and E2. We compute AHPs under the two alternative forcings (Fig. 9) and compare the inter-annual variability of observed production to the inter-forcing variability (Tab. 3). Run-of-river annual potentials exhibit little variation across the different forcings, as the simulated flows of major rivers hosting run-of-river power plants (primarily the Rhone and the Rhine) demonstrate a low sensitivity to precipitation uncertainty (see Fig. E3. Consequently, the inter-forcing variability of simulated potential (defined as the mean standard deviation of annual potential across the forcings) is three times smaller than the interannual variability of run-of-river power production(defined as the standard deviation of observed annual productions), see Table 3. It is also slightly smaller than the modeling error (RMSE of SAFRAN simulated potentials compared to observations), indicating a low sensitivity of simulated run-of-river production to the precipitation uncertainty. Conversely, reservoir plant production shows a much higher sensitivity to precipitation disparities between forcings. Lower COMEPHORE precipitations in mountainous regions lead to an average decrease of 18.7% in the total simulated potential, compared to the SAFRAN simulation. As a result, the variability among forcings is of the same order of magnitude as the interannual variability of production and is higher than the modeling error. Finally, poundage power plants fall in an intermediate category, displaying an inter-forcing variability that is 41% lower than the interannual variability.

In conclusion, the uncertainties in precipitation forcing in mountainous regions prove to be critical in the estimation of realistic hydropower potentials for reservoir plants. The calibration carried out relative to SAFRAN is less effective for other forcings, SAF_COM for instance, as the differences in precipitation data appear as the main contributor to the differences in hydropower potentials.

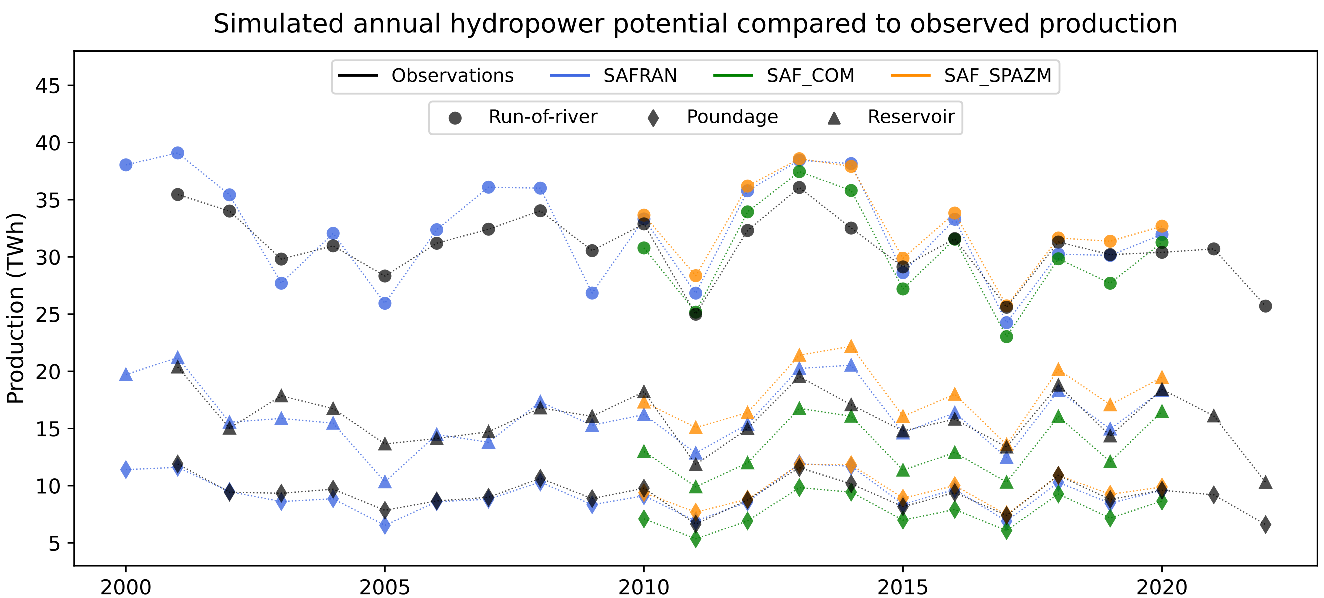

Figure 9. Comparison of estimated annual hydropower potential with observed annual production for the different categories of hydropower plants and for the different atmospheric forcings, after calibration based on SAFRAN.

4.2 Hydropower operations

In this section, we assess the model's ability to simulate reservoir management and hydropower production. Observed time series of river production (gathering run-of-river and poundage power plants) and reservoir production serve as demand inputs for the reservoir operations in the model. At each time step, the model aims to meet this target by operating the reservoirs according to the rules described in Sect. 2.3 and the simulated hydrological cycle. The objective is to verify if our model can simulate operations consistent with observed production. We present here the results obtained from a simulation spanning the period from 2015 to 2020.

	Run-of-river		Poundage		Reservoir	
	Calibration Period	Validation Period	Calibration Period	Validation Period	Calibration Period	Validation Period
Mean relative error	-	+ 2.8 %	-	-2.6 %	-	-1.4 %
Mean absolute relative error	3.5 %	6.9 %	3.7 %	5.4 %	2.5 %	7.5 %
Interannual variability (TWh)	3.71		1.71		2.61	
Inter-forcing variability (TWh)	1.32		1.25		2.54	
Modeling error (TWh)	2.64		0.67		1.33	

Table 3. Estimation of the errors in annual potentials prediction

4.2.1 River production

At each time step, the model first computes the available potential from fatal production (from run-of-river plants and spill or constrained releases from the reservoirs of poundage plants). If this potential falls short of fulfilling the production target, it then operates the reservoirs associated with poundage plants to supplement the production.

Figure 10 details how the simulation compares to the prescribed production throughout the period when forced by SAFRAN. The overall seasonality of the production is quite well reproduced, with the model succeeding in meeting the hourly production target 69.0% of the time. The failures (in red in Fig.10) represent a total volume of 6.9% of the prescribed production over the six years. They mostly occur during summer and fall and indicate that the simulated hydrology is unable to produce what was actually produced during these periods. In winter and spring, however, there are instances when the potential of fatal production is higher than the target production (January and February 2018 for instance), which means that, in the model, more power could have been generated during these periods than was actually observed. These discrepancies are likely due to the discharge seasonality bias in the Rhone and Rhine catchments highlighted in Fig. E4. Despite these discrepancies, the performance of the model remains satisfactory, as it captures gross seasonality and magnitude of run-of-river production, in addition to the inter-annual variability (Fig.9).

Simulation of run-of-river production in the model, when forced by the alternative forcings SAF_SPAZM and SAF_COM, are presented in Fig. C2 and C4. Using SAF_SPAZM, the failures in meeting the prescribed production are reduced (4.3% of production not satisfied compared to 6.9%), due to slightly higher annual potentials of run-of-river and poundage power plants (Fig. 9). On the other hand, with SAF_COM the lower potentials lead to higher failures (15.4% of the total production), consistent with the lower potentials obtained in Fig. 9. However, the seasonality remains very similar in all three simulations, consistent with the similar seasonality of the simulated discharges for the Rhine and Rhone rivers (Fig. E2).

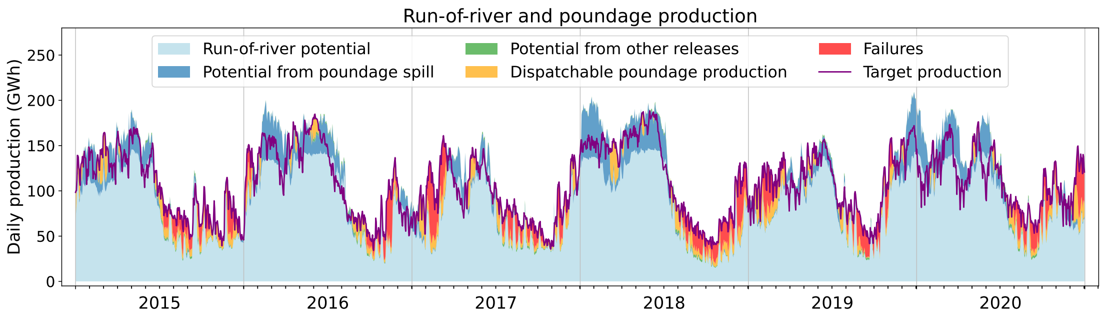

Figure 10. Run-of-river and poundage plants daily production. The purple line indicates the production prescribed to the model and the red coloring shows the failures of the model to meet this target production when forced by SAFRAN. The other colors refer to the nature of the flow that contributes to production in the model. Light blue represents the gross potential of run-of-river plants, dark blue represents the potential of spill from poundage reservoir (water overflowing from the reservoir), green represents the potential from constrained releases of poundage reservoirs and lastly orange represents the dispatchable production, generated by the water specifically released from the poundage reservoirs for power generation.

4.2.2 Reservoir production

Similarly, a 30-minute time series of observed production by reservoir power plants is prescribed to the model. To fulfill this demand, the model completes the non-dispatchable production that may be available from reservoir spillage and constrained releases by operating reservoirs according to the rules defined in Sect. 2.3. Figure 11 details how the simulation compares to the prescribed production throughout the period when forced by SAFRAN. Simulated production under the other forcings is presented in Fig. C3 and C5. Figure 12 displays the co-evolution of the observed national hydraulic stock (RTE, b) and the one simulated in the model (Eq. (17)) for the three forcings under study.

Under SAFRAN, the model successfully meets the production target while simulating hydraulic stock variations consistent with observations throughout the six-year period. Reservoirs are filled during the spring due to snow melt and depleted during the winter to meet the high electricity demand. Nevertheless, a slight temporal shift is observed, as the simulated stock starts to fill some weeks earlier compared to the observations. This temporal shift aligns with the seasonal biases in river discharges identified at the Chamonix Station (Fig. E4), indicating a consistent pattern.

Under SAF_SPAZM, the stock remains significantly higher than the observations. Indeed, the simulated annual potential of reservoir power plants exceeds their observed production (Fig. 9), resulting in reduced releases from the reservoirs to meet the prescribed demand. This leads to high levels of unused spillage, as shown in Fig. C3.

Under SAF_COM, however, the stock is completely emptied after the two first years of simulation, and a significant portion of the demand cannot be satisfied (Fig. C5). This is consistent with the huge difference in annual production estimates highlighted in Fig. 9. In addition to the substantial deficit in hydropower potential, a negative feedback loop comes into play. As the reservoir storage diminishes, the head of the power plants decreases, consequently reducing the associated power generation

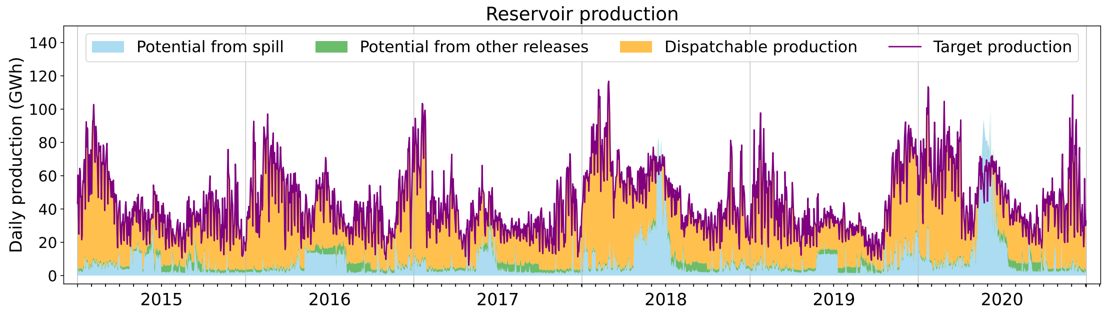

Figure 11. National reservoir plant production simulated in the model. The purple line indicates the production prescribed to the model,while the other colors refer to the nature of the flow that contributes to this production. Blue represents the gross potential from reservoir spillage (water overflowing from the reservoir), green represents the potential from constrained releases of the reservoirs and lastly orange represents the production by the water that is specifically released from the reservoir for hydropower purposes.

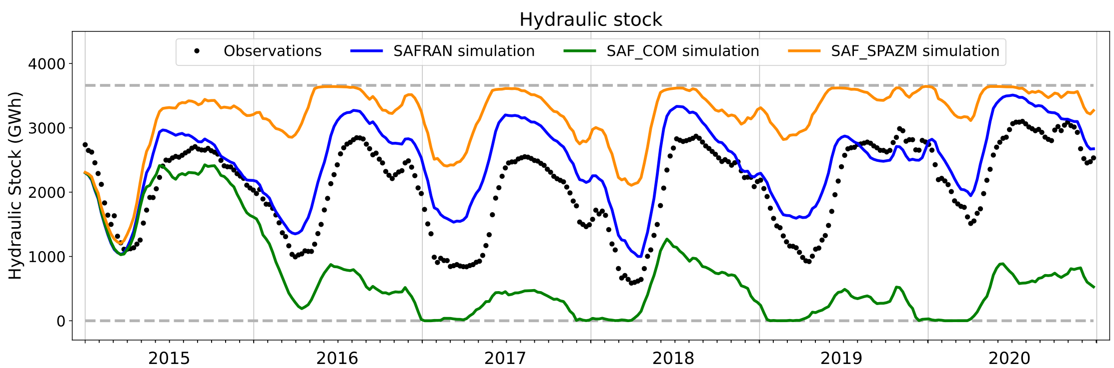

Figure 12. Comparison of national hydraulic stock evolution simulated by the model and weekly observations

for a given released volume. Consequently, the power plants draw more water to generate the same amount of energy, further exacerbating the decline in reservoir storage. The calibration carried out relative to SAFRAN is not effective in avoiding this outcome.

Figure 11 allows for the distinction of the different drivers of French hydropower production, depending on the season. In winter, hydropower production is substantial, driven primarily by high electricity consumption. The majority of production stems from intentional reservoir operations, with a minimal proportion attributed to fatal production. In spring, fatal production becomes more prominent, particularly due to snow melt-induced spillage, resulting in a minimum hourly production, even during periods of low consumption such as at night (only visible at the hourly resolution not displayed here). During summer, although there is no spillage, a significant portion of the hydropower potential comes from constrained ecological and agricultural water releases. When looking at the hourly production (not displayed here), we find a good agreement between the simulated minimal production and the observed troughs in RTE's production.

4.3 Effects of hydropower operations on river discharges

We explore in this section to what extent the representation of hydropower operations can reduce the hydro-meteorological errors of the model discussed in Appendix E, with the example of two gauging stations located in the Alps. Figure 13 details the location of these stations comparatively to the hydropower network. The Aiguebelle station is located on the Arc river, just upstream of its confluence with the Isère river, and downstream from a series of hydropower plants, including one that generates electricity through the release of a dam on the Isère river. The Cheylas station is located on the Isère river, downstream of its confluence with the Arc.

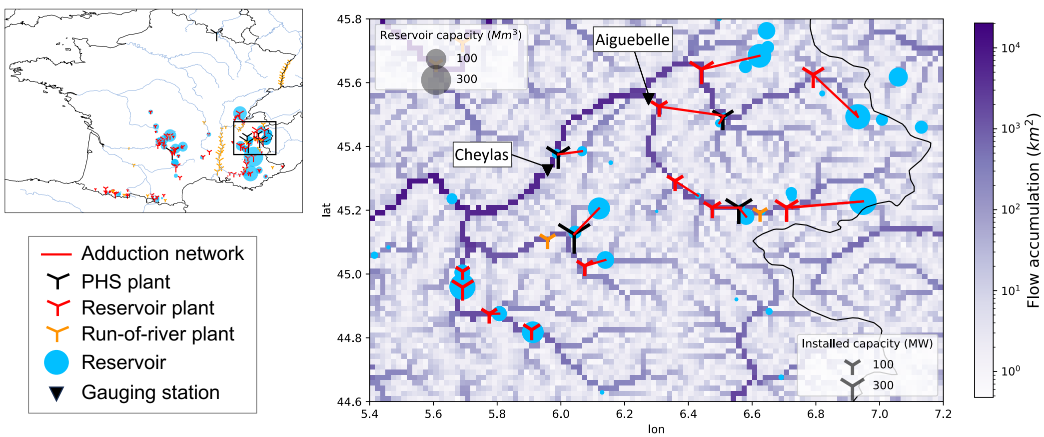

Figure 13. Location of Aiguebelle and Cheylas stations comparatively to hydropower infrastructures in Arc catchment (French Alps). PHS plants are pumped-hydro storage plants not considered in this study.

Figure 14 compares the seasonality of the discharges simulated at these two locations by ORCHIDEE forced by SAFRAN with and without activating the hydropower operations module.

At the Aigubelle station, implementing hydropower operations significantly reduces the annual bias from -31% to -4% (Fig. 14). Indeed, when hydropower operations are activated, a portion of the Isère's water is diverted from its natural outlet to supply a power plant on the Arc. At Cheylas, no change is observed in the bias of the simulated river discharge. Furthermore, the discharge seasonality is improved for both stations with higher flows in Fall and Winter due to releases for power generation. This results in a significant improvement in the NSE metric.

We found a similar effect for other French watersheds where flow observations near hydropower plants are available. However, as mentioned earlier, the professional secrecy surrounding French hydroelectric production complicates a systematic and precise evaluation of this improvement in flow simulation.

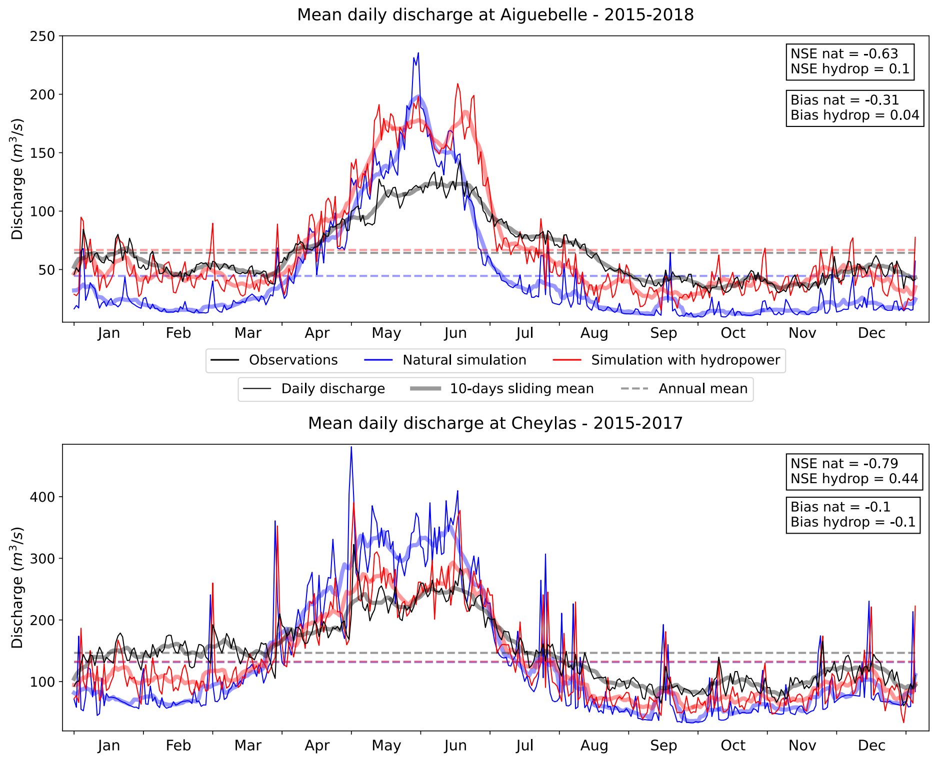

Figure 14. Comparison of daily (fine line) simulated river discharge with hydropower operations (red) and without (blue) and observed discharge (black) for two gauging stations in the French Alps. The thicker line is the 10-day average while the dashed line is the annual mean.

5 Discussion and conclusion

5.1 A demand-based approach

This study demonstrated the effectiveness of a demand-based approach to simulate hydropower operations in land surface models. The conceptual framework of such an approach was first described, emphasizing its three original features: (i) the reconstruction of the human-made hydropower network on the model grid to represent not only natural water flows but also those built for hydropower management; (ii) the implementation of reservoir operation rules that account for their multi-purpose objectives; (iii) the prescription of an exogenous “hydropower demand” defined at the power grid level to drive the release rules of hydroelectric reservoirs, allowing coordinated management of all hydroelectric resources on the power grid and consistent with power system needs. Subsequently, we assessed the performance of this approach when implemented in the routing module of the ORCHIDEE model, for the case study of the French power grid. The ORCHIDEE model was run driven by an atmospheric reanalysis dataset and national historic hydropower production time series were prescribed to the model as the hydropower demand to satisfy. The results indicate that, when the model is forced to reproduce the historic generation, the implemented method simulates hydroelectric reservoir operations in line with observations of reservoir storage at the national level.

Beyond this satisfactory result, our method presents several limitations and opportunities for improvement.

First, the time series used to drive the reservoir releases in this study is the actual production of dispatchable hydropower plants, which may differ from the real demand for dispatchable hydropower production. Indeed, the actual production is the result of a trade-off between the demand and the prevailing hydrological conditions, particularly the current storage level in reservoirs. If this storage is low, the demand will not be fully satisfied in order to maintain a certain level for future uses. Besides, we consider an exogenous dispatch of the hydropower production across the different types of hydropower plants (namely run-of-river and reservoir) at each time step. This approach facilitates the identification of model deficiencies for each type of power plant. For instance, we found a seasonal bias in run-of-the-river hydropower production, that would have been overlooked if a single production target had been used for all power plants. The reservoir plants would have served as buffers, reducing their production during periods of excess run-of-the-river output and increasing it during periods of deficits, thereby resulting in discrepancies in the stock evolution. However, in reality, the dispatch of power demand across the different types of hydropower plants is not exogenous but also depends on the hydrological conditions, as the potential for run-of-the-river production is fully exploited before turning to dispatchable units. To capture these intricate interactions between hydrology and hydropower production decisions, a solution is to couple our model with an economic power system dispatch model (Oikonomou et al., 2022). This coupling would ensure that the power demand dispatch used to drive reservoir operations in ORCHIDEE considers the hydrological states simulated within the ORCHIDEE model. This would result in a comprehensive modeling framework wherein simulated hydropower production simultaneously adheres to constraints related to water availability, non-power reservoir operations, and minimization of power system costs. In particular, hydropower demand would be endogenously adjusted to match the hydropower potentials of the simulated hydrology and could avoid entering the feedback loop where reservoirs are emptied, as in the SAF_COM simulation. This novel approach holds significant promises for enhancing the consistency and realism of hydropower production simulation, in particular the study of the joint impacts of climate change and variable renewable energy integration.

Second, in this study, we opted for a simple rule to distribute national production among different power plants and demonstrated that such a rule could simulate credible hydroelectric operations at the national level. As no time series of production is available at the individual plant level in France, the realism of the simulated individual operations is difficult to assess. This choice can, however, be further investigated, in particular by testing alternative distribution rules, such as those proposed by Lund and Guzman (1999). Additionally, the operations we simulate assume that a social planner controls the entire grid's power plants and reservoirs, optimizing the collective production. In reality, power plants may belong to different stakeholders, each seeking to maximize their profit. Ambec and Doucet (2003) have shown that such decentralized management can lead to suboptimal resource management, which could not be reproduced by the proposed model. However, in the case of France, our assumption is justified as the historical production company, EDF, owns nearly 85% of the hydroelectric production.

Third, as we focused primarily on hydroelectric usage, other water uses are simplified or even absent in the current version of our model. Specifically, no water abstraction for domestic, industrial, or agronomic needs is included in our model. Following

Zhou et al. (2021), the irrigation demand could be explicitly calculated by the model based on the deficit between potential evaporation and actual evapotranspiration. In other studies, domestic and industrial water demands are estimated using socio-economic proxies such as population density or GDP (Neverre, 2015).

5.2 Sources of uncertainties

We have paid particular attention to identifying and discriminating among the various sources of uncertainty that may affect the estimation of hydroelectric production using such a method. Our findings indicate that while errors in simulated discharge are prevalent in most watersheds in our case study, the limited knowledge of the hydroelectric adduction network is the main source of uncertainty for hydropower infrastructures in mountainous basins. To our knowledge, no dataset comprehensively documents these complex "hydroelectric links", which operate on a small scale. Therefore, an in-depth analysis of the gray literature released by the various stakeholders is necessary to reconstruct this network in detail. Furthermore, we proposed a calibration method to overcome this limitation and validated it against observations for the case study of France. This method can therefore be extended to countries with limited information available on the hydroelectric network.

Regarding hydro-meteorological errors, the use of three different precipitation datasets allows us to understand their more precise origin. In several watersheds crucial for hydroelectricity (such as Durance or Lot), and especially in the upstream parts, uncertainties in observed precipitation appear to be the primary contributor to the error in simulated discharge. On the Rhone or the Rhine rivers, on the contrary, errors in the simulated discharges seem to stem more from processes not represented in the model (such as water withdrawals for human uses, for example). Though incomplete, this work contributes to the current effort to integrate human water management into hydrological models, in order to simulate a more realistic water cycle (Nazemi and Wheater, 2015a). We show that our method can improve river flow simulations in some mountain catchments where hydropower cannot be neglected.

Finally, our study shows that comparing hydropower estimates with observed production offers an indirect means of checking the quality of meteorologic data. In our study case, we demonstrate the lower quality of the COMEPHORE dataset in mountainous regions compared to SAFRAN or SPAZM, something already identified by Birman et al. (2017); Magand et al. (2018).

5.3 Perspectives

In conclusion, the demand-based operations proposed in this study hold promising prospects for enhancing our understanding of the resilience of different power mix scenarios to changes in climate, water management, or land use. The next steps in this trajectory involve (i) integrating our climate-based hydropower model with a power system model to get a comprehensive framework that captures all relevant constraints on hydropower production, (ii) applying this integrated framework to climate change scenarios and power system scenarios to assess the adaptive capacity of the power grids, and (iii) refining the description of other water uses to more completely describe the competition for water resources.

Code and data availability. The ORCHIDEE version developed for this project is available upon request. The meteorological forcings used in this study were provided by Meteo-France for SAFRAN (https://www.umr-cnrm.fr/spip.php?article788&lang=en) and COMEPHORE (https://radarsmf.aeris-data.fr/en/home-page/), and EDF-DTG for SPAZM (Gottardi et al., 2008)). The observed data used for validation is openly accessible online. River discharge data can be downloaded at https://hydro.eaufrance.fr/, while data on energy production is available at https://opendata.reseaux-energies.fr/. The reservoir dataset was built based on the GRanD database (Lehner et al., 2011), which can be found at https://www.globaldamwatch.org/grand/, and on the data of the *Comité Français des Barrages et Réservoirs* (CFBR) at https://www.barrages-cfbr.eu/-En-France-. Finally, the plants database was built from the EU JRC hydro-power plants database (https://github.com/energy-modelling-toolkit/hydro-power-database) and the *Registre national des installations de production raccordées au réeau de transport d'électricité*, which can downloaded at https://opendata.reseaux-energies.fr/.

Appendix A: Building the routing network

A1 Locating hydroelectric infrastructures on the river network

Dams and hydropower plants are located on the MERIT grid based on georeferenced and upstream area information provided in the databases. The infrastructure datasets used for our study over France are presented in Appendix B. The location procedure is done following these steps:

1. The initial location is identified based on geographical coordinates.

2. A search area is defined around this initial location (typically 10km in radius)

   – If the upstream area of the infrastructure is included in the databases, we identify all the pixels in the search area with an upstream area that is close enough to the area being searched (typically +/- 20%). Among these eligible pixels, the one closest to the initial location is selected. If no pixel meets this criteria, the infrastructure is not placed.

   – If no upstream area data is included in the databases, we look for the closest pixel to the initial location that is likely to be situated on a river. To do this, the maximum upstream area of the pixels in the search area is identified (U_{max}) and the closest pixel to the first guess pixel satisfying ($U > \frac{U_{max}}{10}$) is selected, with U being the upstream area of the pixel.

Note that each vertex and edge can respectively contain only one dam or hydropower plant. If several reservoirs are placed on the same HTU during pixel aggregation, their respective volumes for the different uses are summed. If two plants are placed on the same edge, their installed power capacity and head are summed only if both plants have the same input point. Otherwise, only the plant with the highest installed capacity is kept. As in other studies (Abeshu et al., 2023), all the reservoir attributes are associated with the HTU of the dam (even if its water surface can be larger than the HTU area and its geometry is different from the HTU geometry).

A2 Adduction network

Poundage and reservoir plants generate electricity from the water released from the upper reservoirs. To explicitly represent this adduction network in our model, we have to identify such connections between a feeding reservoir and a power plant. Since datasets describing these connections are rarely available, we use an algorithm to identify these connections. For each poundage or reservoir plant, we thus select as the feeding reservoir the one that maximizes the potential function $\phi = \frac{U*V*h}{d}$, where U is the upstream area of the dam, V is the storage capacity of the reservoir, h is the elevation difference between the plant and the reservoir and d is the horizontal distance between them. The definition of these potential functions is inspired by similar works aiming to connect an irrigated area to a water supply point (Neverre, 2015; Zhou et al., 2021).

This position algorithm relies on the assumption that each plant is fed by only one reservoir. This assumption is however debatable, especially for plants in mountain areas that may be connected to several reservoirs. In this case, our choice of the potential function ϕ privileges the reservoir with the largest upstream area since it is likely to determine the production potential of the plants. During calibration (see Sect. 2.5), plants for which the identification of a single reservoir conducts to a significant misrepresentation of the plant's hydropower potential are identified and a correction is made by moving the withdrawal point so that it gathers enough water to ensure the observed production is possible.

Appendix B: Datasets

B1 Dams and reservoirs

We use global reservoir data from GRanD (Global Reservoirs and Dams) dataset (Lehner et al., 2011), which gathers data of large reservoirs and dams worldwide (volume $> 0.1km^3$, hence a total of 7320 dams). The database contains 137 dams in France, 63 of which are used for hydroelectricity. However, some important dams for French hydroelectricity are not documented in this database. Therefore we completed the database for this study with data from the CFBR (Comité Français des Barrages et des Réservoirs), which is in charge of the inventory of French dams higher than $15m$ for the ICOLD (International Commission on Large Dams). We extracted data from its website (CFBR, 2021) to complete the GRanD database. Our database finally gathers 492 French dams. Their location, original database, and intended purposes are shown in Fig. B1.

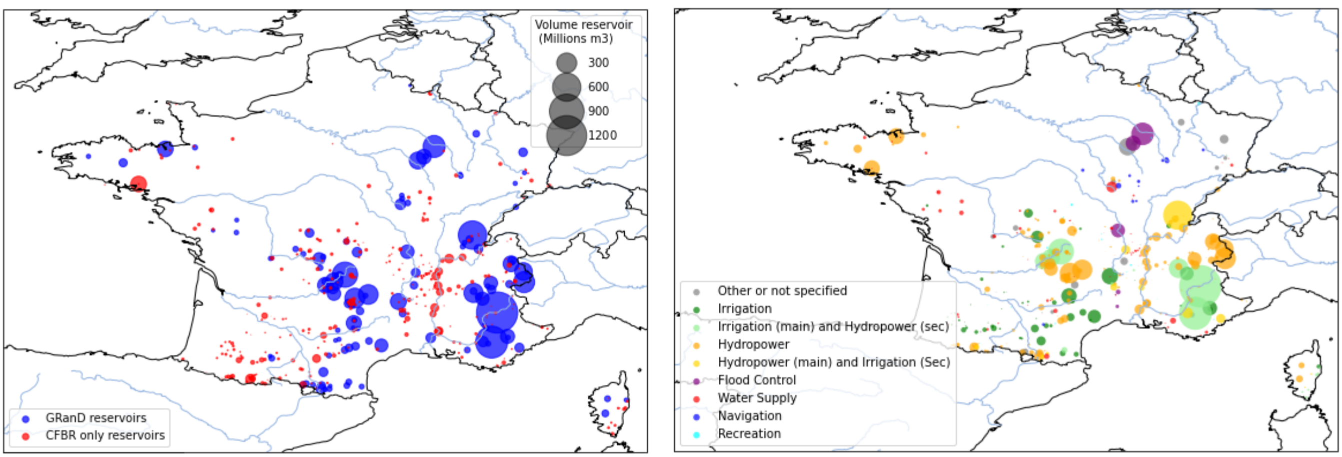

Figure B1. Location and main uses of the reservoirs in the final database

B2 Hydropower plants

The data used in this study are obtained from the EU Joint Research Center Hydro-power plants database (European Commission and Joint Research Centre (JRC), 2019). This database gathers geographical coordinates, installed power capacity, plant type (run-of-river, reservoir, or pumped-hydro storage (PHS)), and hydraulic head for 4186 European plants (for a total installed capacity of 161 GW). 153 of these plants are located in France, representing 20.6 GW. Other available datasets of French hydropower plants are the national registers of electricity generation and storage facilities published annually (ODRÉ, 2016, 2018). The 2016 register gathers data from 414 hydropower plants, with a total installed capacity of 23.4 GW. However, as these registers do not provide the geographical coordinates of the plants, we chose to use the JRC database. Nevertheless, we use data from the 2016 national register to rectify head information and categorize the plants in the 4 categories used by the French operator: run-of-river, poundage, reservoir, and PHS. Figure B2 shows the locations of the plants included in our final database, while Table B1 summarizes the discrepancies between the databases in terms of installed capacities.

	Total	Run-of-river	Poundage	Reservoir
National Register 2016 (ODRÉ, 2016)	23.426	5.943	3.715	8.748
JRC (initial categories)	19.695	5.87	-	8.76
Final database (plants from JRC database, classified following RTE categories which have been located on HTUs)	19.638	4.426	2.606	7.434
compared to ODRÉ (2016)	*84.6%*	*74.2%*	*71.7%*	*86.0%*

Table B1. Comparison of the different databases in terms of installed hydroelectric capacities (GW) in metropolitan France (without Corse et DOM-TOM)

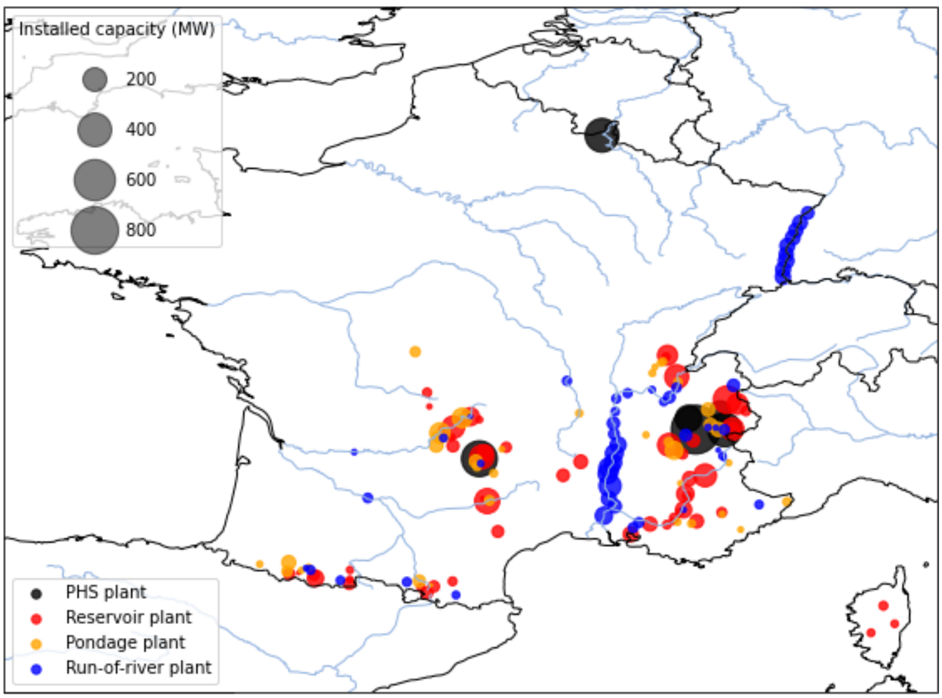

Figure B2. Typology of the plants in the database

B3 Conversion factors for hydropower generation

As presented in Table B1, our final dataset does not include all the hydropower plants installed in France. However, using annual production data of each plant provided by ODRÉ (2015, 2016, 2018), we can quantify the share of the national production provided by the power plants in our database. This enables us to compute a factor to convert the actual production of national time-series (RTE, a) into representative production in our model both for prescribing the production demand and comparing the results. The computation of such conversion factors is presented in Table B2. It relies on the assumption that within each category of power plant, the geographical distribution of plants in our database is representative of all French power plants so that production ratios remain constant over time. This assumption is debatable as our database includes the largest power plants in terms of installed capacity, which are predominantly concentrated in certain regions, while smaller-scale plants may be located in watersheds not represented in our database (e.g., run-of-river plants on the River Seine for instance). However, as the missing plants have, by definition, a lower installed capacity than those in our database, their contribution to national production is lower and can reasonably be neglected.

	Total	Run-of-river	Poundage	Reservoir
National production in 2016 (RTE et al., 2016)	62.6	31.6	9.4	15.8
Total production from plants in national register in 2016 (ODRÉ, 2016)	57.6	27.5	9.0	15.6
compared to RTE et al. (2016)	*92.0%*	*87.0%*	*95.7*	*98.7%*
Total production from plants in the database in 2016 (based on ODRÉ (2016))	47.9	22.4	5.5	14.1
Coefficients 2016		70.9%	58.5%	89.3%
National production in 2018 (RTE et al., 2018)	66.9	31.3	10.9	18.8
Total production from plants in national register in 2018 (ODRÉ, 2018)	60.7	26.4	10.0	18.3
compared to RTE et al. (2018)	*90.7%*	*84.3%*	*91.7%*	*97.3%*
Total production from plants in the database in 2016 (based on ODRÉ (2018))	48.1	20.5	6.0	16.2
Coefficients 2018		65.5%	55.0%	86.1%
Conversion factors		**68.2%**	**56.8%**	**87.7%**

Table B2. Comparison of the different available databases in terms of annual production (TWh) and calculation of conversion factors. n.a.=not available

Appendix C: Alternative precipitation datasets

C1 Presentation of the datasets

C1.1 COMEPHORE

COMEPHORE (COmbinaison en vue de la Meilleure Estimation de la Précipitation HOraiRE) dataset provides observations of surface precipitation accumulation over metropolitan France at an hourly and kilometric resolution based on a synthesis of radar and rain gauge data. A specific processing chain has been implemented in order to address the various sources of error affecting radar data, in particular its low quality in high altitude mountainous areas like the Alps or the Pyrenees (Fumière et al., 2020). The final database is nevertheless assumed to be the best representation of surface precipitation over metropolitan France (Fumière et al., 2020).

We build a meteorologic dataset SAF_COM by replacing precipitation data in SAFRAN with data from COMEPHORE. As COMEPHORE does not distinguish solid and liquid precipitations, we keep SAFRAN's hourly ratio of solid/liquid precipitations when possible and discriminate based on the air temperature otherwise.

The differences in annual mean precipitation are generally small between SAFRAN and COMEPHORE, with an average deviation inferior to 1.0% in COMEPHORE compared to SAFRAN (Fig. C1). However, we find a small seasonal bias as this average deviation goes from -2.0% for the Winter period to +1.9% in the Summer. Moreover, discrepancies increase dramatically in mountainous regions, especially in the Alps and the Pyrenees. For grid points with an average elevation above 1000m, the annual mean precipitation in COMPEHORE is, on average, 10.4% lower.

C1.2 SPAZM

SPAZM (SPAtialisation des précipitations en Zone de Montagne) is a daily reanalysis of precipitation at the kilometer scale, developed by EDF, the main electricity producer in France. SPAZM specifically covers the southern half of the French territory, where a large majority of hydroelectric power plants are located (Gottardi et al., 2008). Climatological precipitation outlines are first constructed based on daily precipitation observations categorized by types of oceanic circulation (weather patterns) (Garavaglia et al., 2011). These outlines are then spatially interpolated onto the kilometer-scale grid and deformed daily according to available observations. In addition to Météo-France's observations, which are also used to construct SAFRAN, EDF's measurement network is utilized. We interpolate the daily precipitation data from SPAZM to the hourly scale and merge it with SAFRAN data to create the alternative forcing dataset SAF_SPAZM. As for SAF_COM, we keep SAFRAN's hourly ratio of solid/liquid precipitations when possible. Compared to SAFRAN, precipitations are in average 2.7% higher in SPAZM with an average bias of 7.0% in Summer, against 2.1% in Winter. Bias is heterogeneously spread over France (Fig. C1) with bigger differences on the highest reliefs, without a clear sign (average deviation of +3.9% for grid points above 1000m).

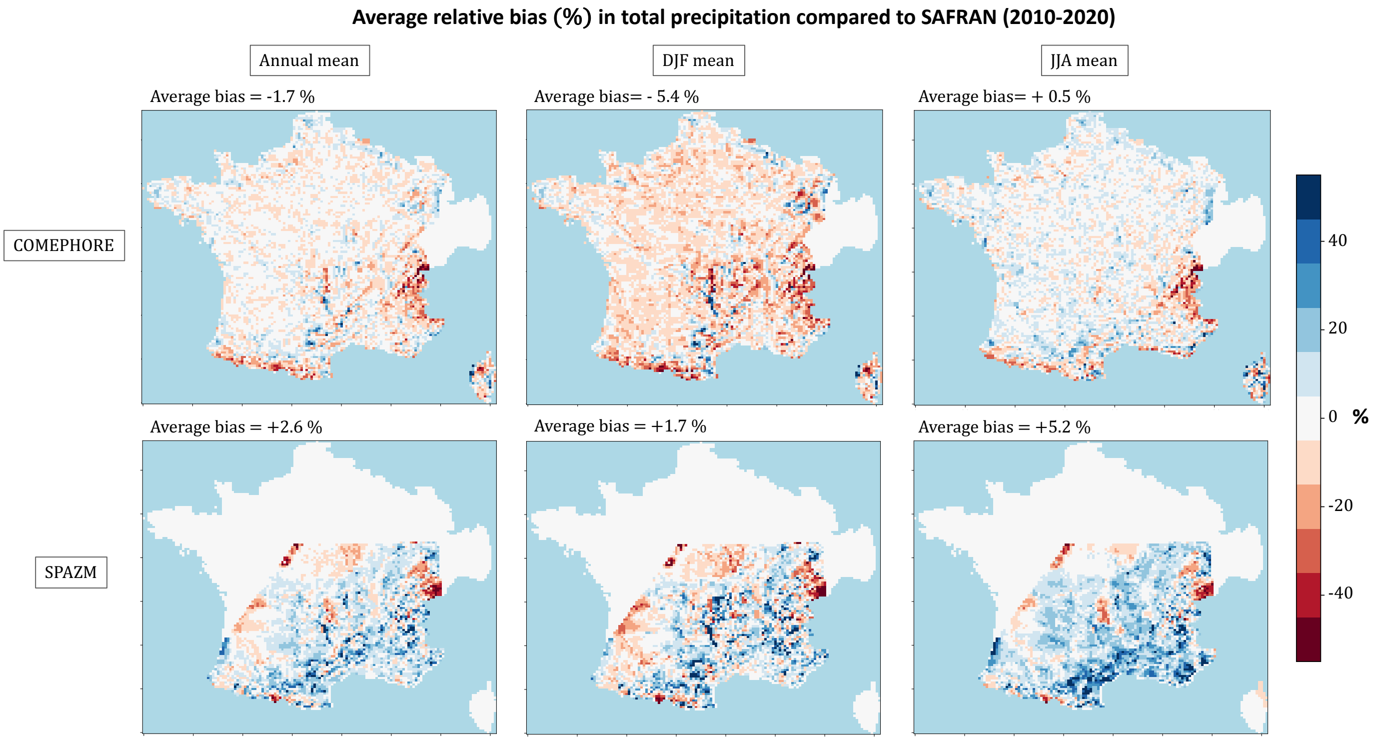

Figure C1. Average relative differences in total precipitation across the datasets for the period 2010-2020.

Left column: annual average bias, middle: average bias in Winter period (December-January-February), right: average in Summer period (June-July-August)

Top: COMEPHORE dataset compared to SAFRAN, Bottom: SPAZM compared to SAFRAN

C2 Simulation of hydropower production under SAF_SPAZM

C3 Simulation of hydropower production under SAF_COM

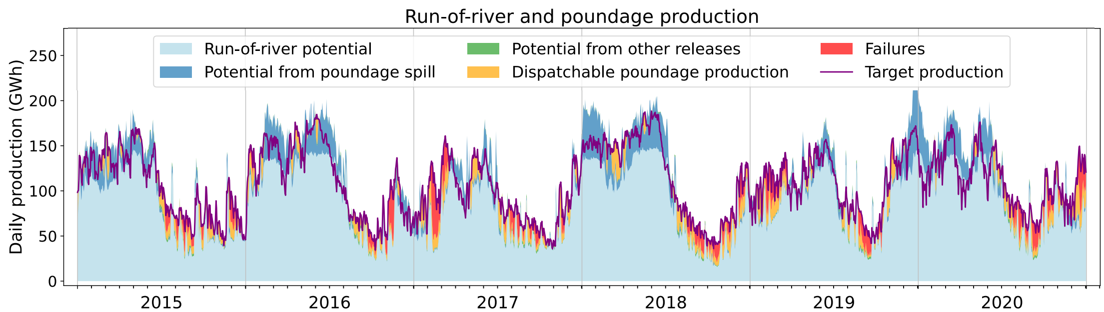

Figure C2. National run-of-river plant production simulated in the model when forced by SAF_SPAZM. The purple line indicates the production that has been prescribed to the model and the red shows the difference between this production and the one simulated in the model when forced by SAF_SPAZM. The other colors refer to the nature of the flow that contributes to the production in the model. Light blue represents the gross potential of run-of-river plants, dark blue represents the potential of spill from poundage reservoir (water overflowing from the reservoir), green represents the potential from constrained releases of poundage reservoirs and lastly orange represents the dispatchable production, generated by the water specifically released from the poundage reservoirs for power generation.

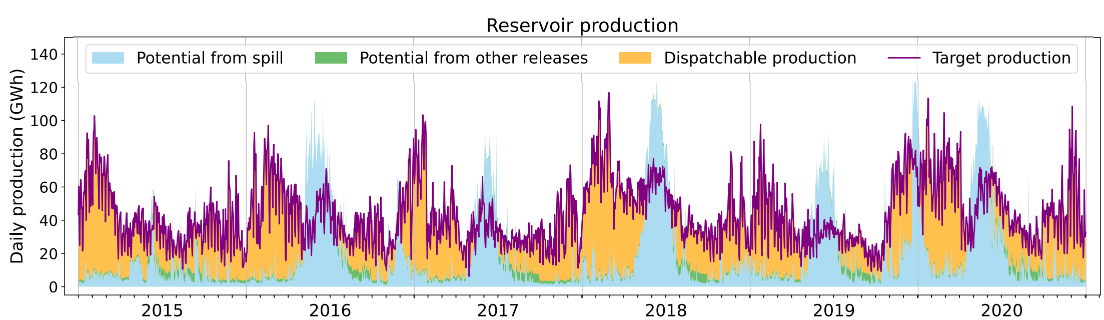

Figure C3. National reservoir plant production simulated in the model when forced by SAF_SPAZM

The purple line indicates the production that has been prescribed to the model.The other colors refer to the nature of the flow that contributes to this production. Blue represents the gross potential from reservoir spill (water overflowing from the reservoir), green represents the potential from constrained releases of the reservoirs and lastly orange represents the production by the water that is specifically released from the reservoir for hydropower purposes.

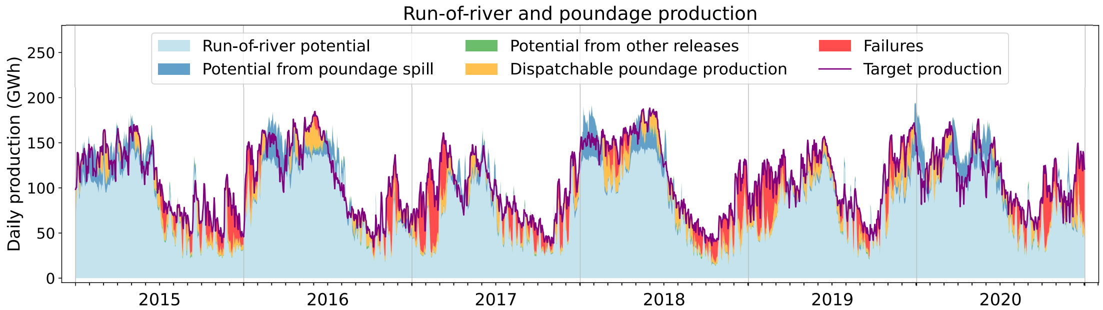

Figure C4. National run-of-river plant production simulated in the model when forced by SAF_COM. The purple line indicates the production that has been prescribed to the model and the red shows the difference between this production and the one simulated in the model when forced by SAF_COM. The other colors refer to the nature of the flow that contributes to the production in the model. Light blue represents the gross potential of run-of-river plants, dark blue represents the potential of spill from poundage reservoir (water overflowing from the reservoir), green represents the potential from constrained releases of poundage reservoirs and lastly orange represents the dispatchable production, generated by the water specifically released from the poundage reservoirs for power generation.

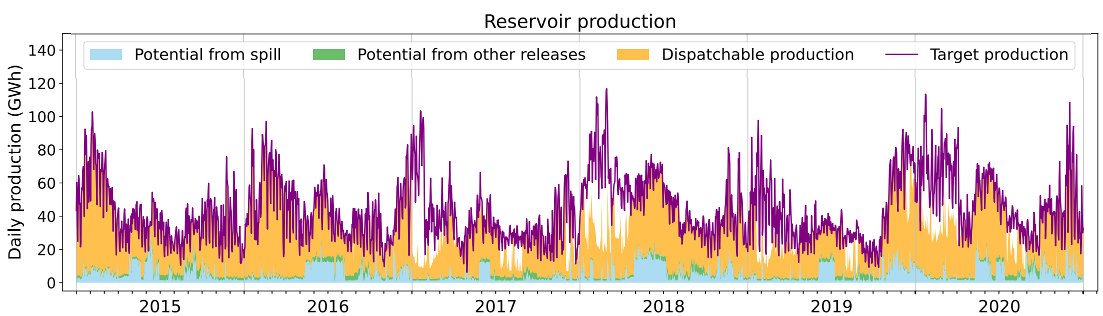

Figure C5. National reservoir plant production simulated in the model when forced by SAF_COM
Purple line indicates the production that has been prescribed to the model.The other colors refer to the nature of the flow that contributes to this production. Blue represents the gross potential from reservoir spill (water overflowing from the reservoir), green represents the potential from constrained releases of the reservoirs and lastly orange represents the production by the water that is specifically released from the reservoir for hydropower purpose.

Appendix D: Hydropower network error

The La Bathie power plant is the most important reservoir hydropower plant in France in terms of installed capacities. It is located in the Alps and fed by numerous water intakes, as illustrated in Fig. D1. Among them, are the reservoirs of Roselend, Saint Guérin, and La Gittaz as well as other intakes directly connected to rivers or glaciers.

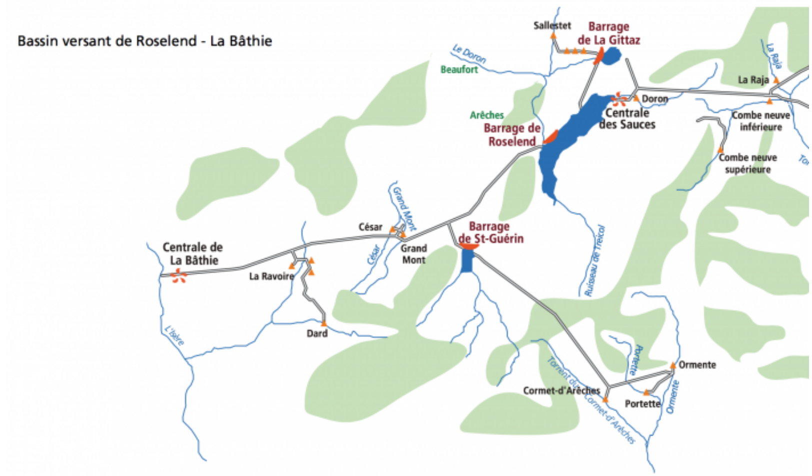

Figure D1. Schematic representation of the water aduction network to La Bathie power plant (source:vpah-auvergne-rhone-alpes.fr)

Figure D2 describes the same area in HTUs space and shows that the Roselend reservoir accounts for only a small part of the water being transferred to the hydropower plant.

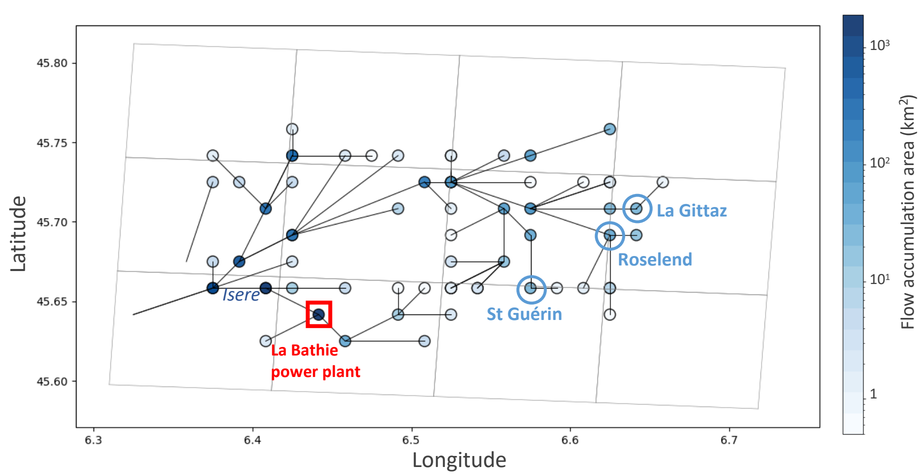

Figure D2. HTUs representation in the model for the same spatial area as Figure D1. The location of hydropower infrastructures is indicated.

Appendix E: Hydro-meteorological errors

To evaluate the performance of the ORCHIDEE model to simulate river discharges in France, independent of reservoir operations, we compare daily river discharges simulated by the model with the observations database of Schapi (2022). It is important to acknowledge that the observed discharge data represents actual discharge values, including water withdrawals, while at this stage, ORCHIDEE generates natural discharges without such withdrawals and dam operations.

E1 Bias in average discharge

Figure E1 displays relative biases of average discharge simulated by ORCHIDEE forced by SAFRAN over the 2010-2020 period for a selection of gauging stations located on rivers equipped with hydropower infrastructure (see Fig. B2 for the detailed locations of the power plants). We chose the bias metric because the annual mean discharge is the most relevant parameter for hydropower potential.

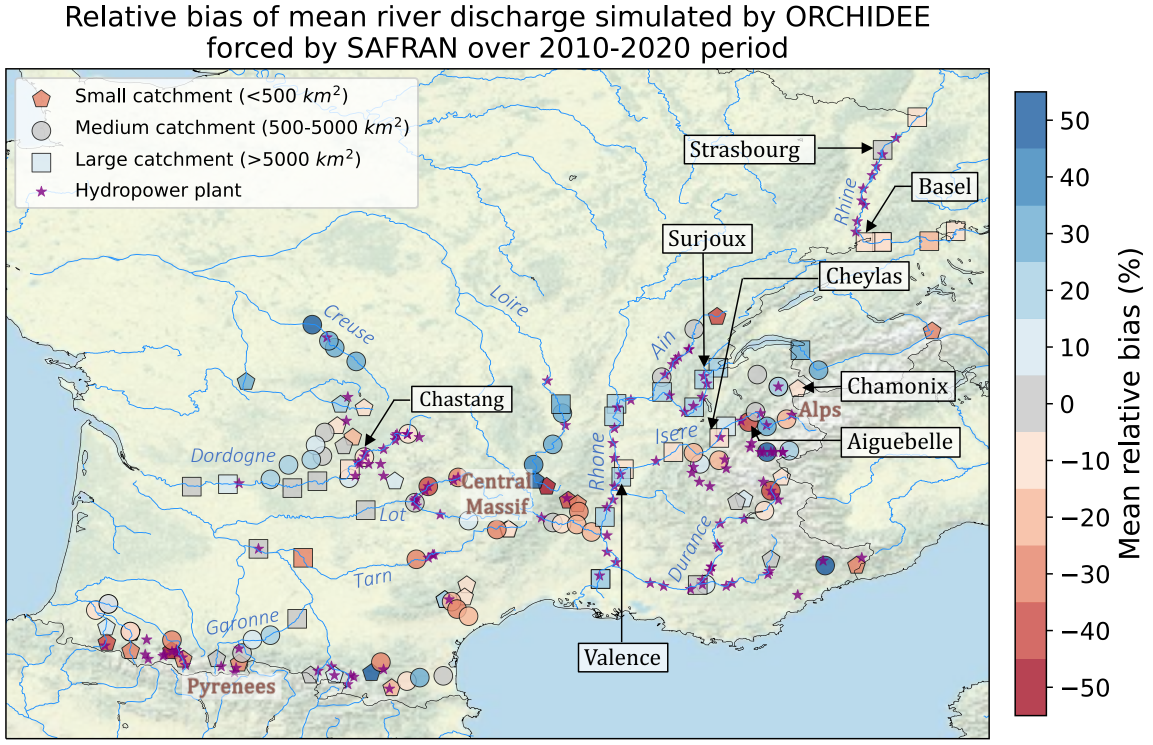

Figure E1. Relative bias of average discharge for a selection of gauging stations located on French rivers equipped for hydropower for the period 2010-2020. Each colored point represents a gauging station, with the shape indicating the size of the concerned watershed, while the color indicates the calculated bias at this location. Purple stars indicate the locations of the hydropower plants located on the model grid. Source: authors, based on a layer by U.S. National Park Service

The overall performance of the model indicates a slight overestimation of flows, with an average bias of +2.4%. The discharge bias shows an increasing trend with the upstream area of stations. For small catchments (less than 500 km^2), the average bias is -1.6%. In medium-sized catchments (between 500 and 5000 km^2), the bias decreases to +1.1%. In large catchments (more than 5000 km^2), the bias becomes more pronounced, reaching 7.6%. It is, however, important to note that the smaller the upstream area, the greater the uncertainty in the location of the station. In Fig. E1, only the stations located with an error in the upstream area lower than 20% are displayed.

On the largest rivers (Rhine and Rhone), where most run-of-river power plants are located, the bias shows little spatial variability, constant at around +20% for the Rhone and -10% for the Rhine respectively. In the Alps, on the other hand, where a significant proportion of dispatchable hydroelectric capacity is installed, the bias displays a high spatial heterogeneity, sometimes within the same river. Upstream of the Isere river, the bias varies from -19% to +26% between two stations some twenty kilometers apart. The upstream reaches of the Durance also show negative biases. In the other massifs equipped for hydroelectricity (the Pyrenees and Massif Central), there are also negative biases at altitude, which gradually diminish downstream.

Assuming negligible observational errors, discharge bias can originate from different error sources:

- Errors in the atmospheric forcing applied to ORCHIDEE;
- Modeling errors in the energy, water, and carbon cycles;
- Missing processes in ORCHIDEE like glacier melting, interactions with groundwater, and water withdrawals).

To explore the first hypothesis, Fig. E2 compares discharges simulated by ORCHIDEE using the two alternative forcings (SAF_COM and SAF_SPAZM) with the reference SAFRAN simulation. The relative biases of these simulations to observations are presented in Fig. E3.

Under SAF_COM, simulated discharges show relatively small differences on annual average, except in mountainous watersheds (Alps and Pyrenees), where the lower precipitation in COMEPHORE results in streamflows that are 30% to 40% lower when compared to the SAFRAN simulation. However, a pronounced seasonal pattern is observed. The simulated streamflows in winter are lower in the simulation forced by COMEPHORE across France (averaging -16% and up to -50% for the Loire and Durance rivers), while in summer, they are higher (averaging +25% and up to +50% for the Loire River). As regards comparison with observed flows (Fig. E3, the negative biases existing under SAFRAN in the Alps and Pyrenees are accentuated, particularly along the Durance and Isere rivers where many hydroelectric power plants are located. However, for some Alpine stations and the Massif Central, for which the flow is overestimated with SAFRAN, the flow is more accurately simulated with COMEPHORE.

Under the SAF_SPAZM forcing, river discharges show an increase in the majority of watersheds, which is consistent with the previously highlighted higher precipitation in this dataset. However, the upper Rhone watershed stands out with a decrease in simulated discharge, reaching up to -40% during the summer season, allowing for a reduction in the bias of simulated discharges in this area.

Even if we limit our analysis to the precipitation variable without considering other forcing variables, we show a significant influence of the forcing variability on the simulated discharges.

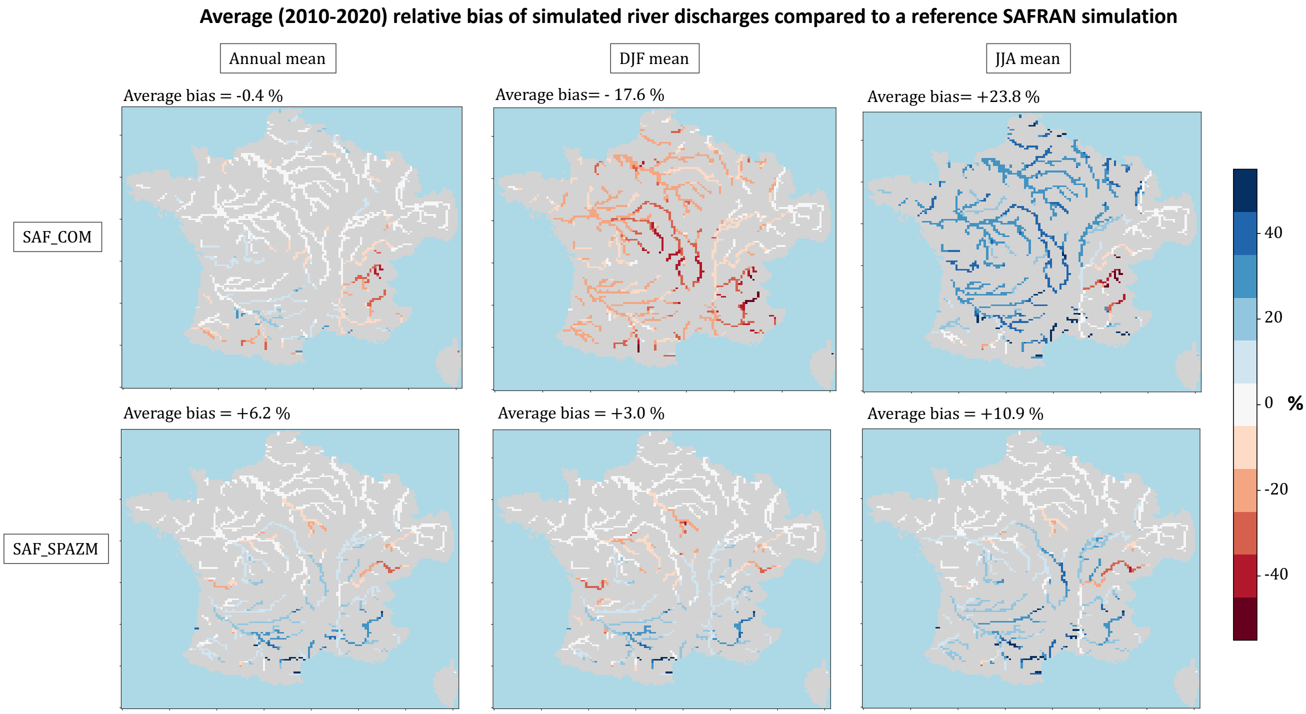

Figure E2. Average relative bias in discharge simulated by ORCHIDEE under alternative precipitation forcings. Results are given in relative difference compared to the reference SAFRAN simulation, for the period 2010-2020. Left: annual average bias, middle: average bias in the Winter period (December-January-February), right: average in the Summer period (June-July-August). The discharges are displayed for all grid points with an upstream area higher than 1000 km^2.

E2 Discharge seasonality

Beyond the bias in average values, the performance of ORCHIDEE in reproducing the seasonality of the discharge is key for the modeling of run-of-river production as well as that of poundage power plants, which have only a very limited storage capacity. Observations and simulations of daily discharges under SAFRAN forcing are presented in Fig. E4 for selected gauging stations in catchments equipped with run-of-river or poundage power plants.

As depicted in Fig. B2, run-of-river plants are mostly located along the Rhone and Rhine rivers. In the upper Rhone (Surjoux station), there is a substantial overestimation of high flows and an underestimation of low flows. The error reduces progressively downstream: the Nash Sutcliffe efficiency (NSE) is better at the Valence station, despite a higher overall annual bias (likely due to the non-representation of water withdrawals). On the Rhine (Basel and Strasbourg stations), we see similar errors, with an underestimation of low flows during the Fall and an underestimation of the Spring maximum. The discrepancy in the Rhone's seasonality can be attributed to the non-representation of Leman reservoir management in our model, which is known to play a crucial role in shaping discharge seasonality in the upper Rhone (Habets et al., 1999).

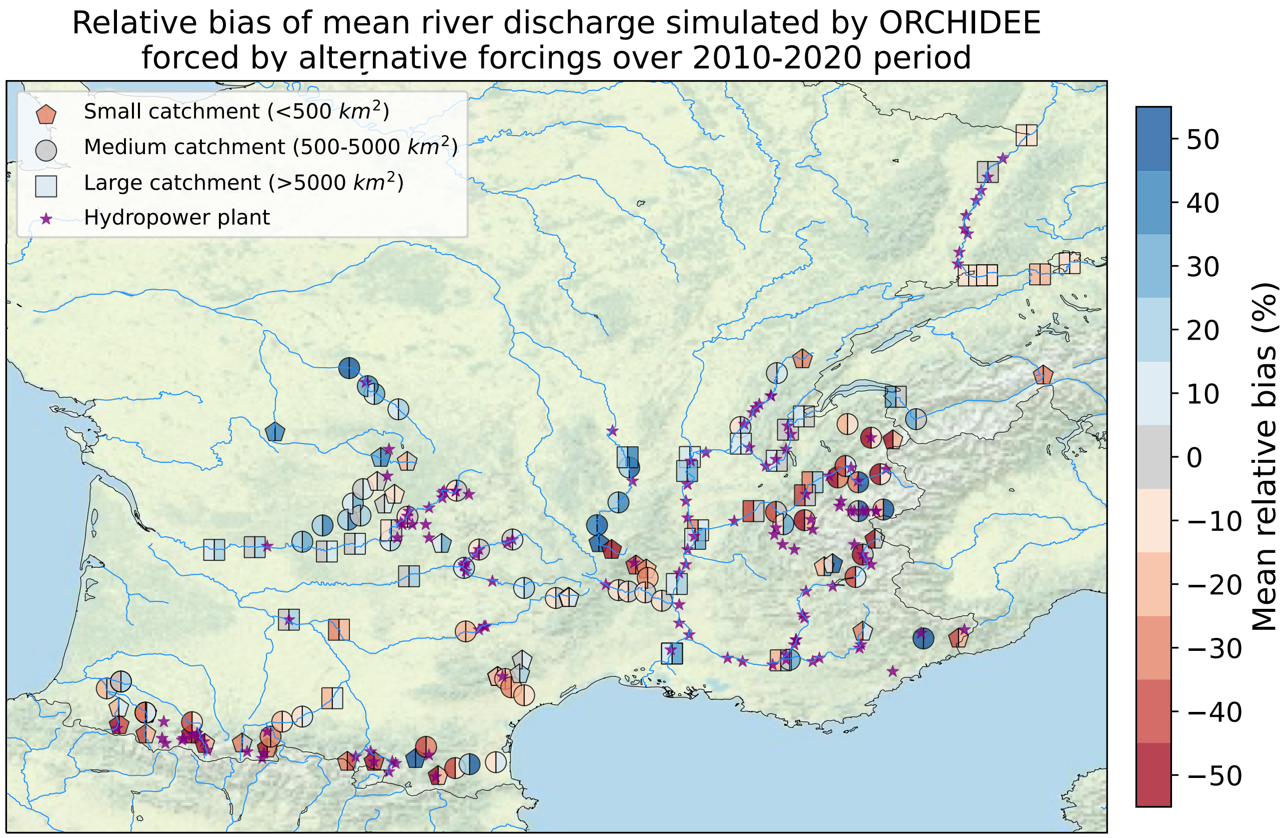

Figure E3. Relative bias of average discharge simulated by ORCHIDEE under alternative forcings for a selection of gauging stations located on French rivers equipped for hydropower for the period 2010-2020. The left coloring indicated the average bias of discharges simulated under SAF_COM while the right coloring indicated the average bias of simulations under SAF_SPAZM.
Source: authors, based on a layer by U.S. National Park Service

Poundage plants are distributed across various catchments. Some of them are concentrated in the upper Dordogne river, notably the Chastang plant, the most powerful poundage facility, which benefits from a gauging station at its location. We find a positive NSE for this station, indicating that the seasonality is well captured by the model.

Finally, some run-of-river and poundage plants are also concentrated in the Alps, where we focus on two gauging stations: Chamonix, situated in a small upper catchment, close to a run-of-river plant and Cheylas, positioned on a large river (l'Isère), downstream from several power plants. At Chamonix, we find a seasonal bias as the model simulates an earlier discharge peak compared to observations (around 2 months ahead). At Cheylas, the model overestimates the seasonal variability of the discharge, with higher flows during Spring and lower flows during Winter, which can be attributed - at least in part - to the non-representation of reservoir management at this stage of our study (see Sect. 4.3).

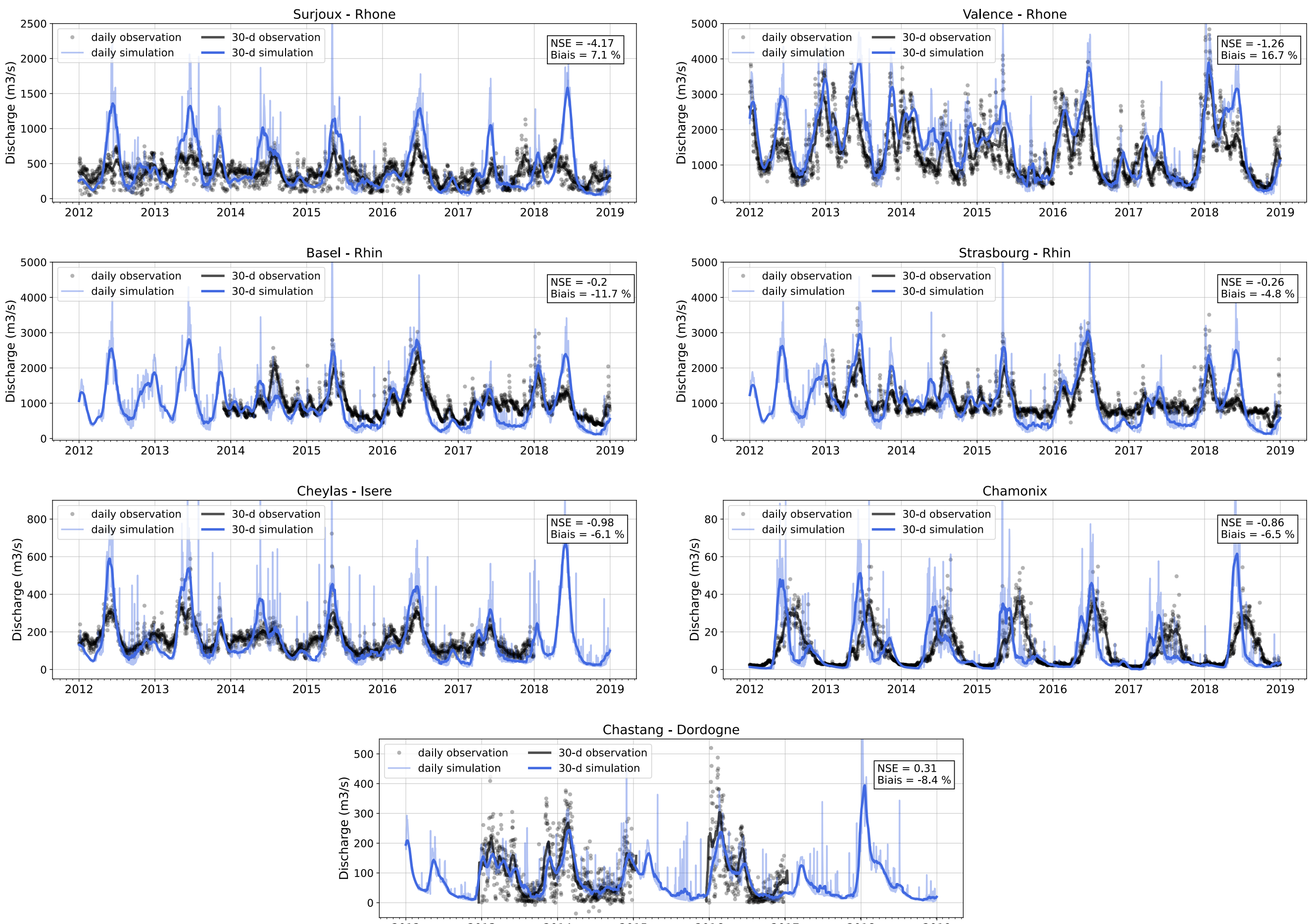

Figure E4. Comparison of simulated and observed river discharges for a selection of gauging stations. Locations of selected stations are indicated in Figure E1. Fines lines and dots are daily time series while ticker lines are 30-day sliding averages. NSE metrics are computed on a daily time series.

Author contributions. LB developed the code, designed and executed the numerical evaluations, and wrote the first draft of the manuscript. JP, PD and PQ supervised the study. All authors jointly discussed the methodology, interpreted the results and improved the manuscript.

Competing interests. The authors declare that they have no conflict of interest.

Acknowledgements. Baratgin's PhD is supported by the French Ministry of Agriculture. The authors are grateful to EDF-DTG for providing the SPAZM precipitation data and to Meteo-France for providing SAFRAN and COMEPHORE data. HydroPortail and ODRÉ are thanked for collecting and distributing respectively the discharge and power production data. IPSL's MesoCentre is thanked for the computer time.

References

Abeshu, G. W., Tian, F., Wild, T., Zhao, M., Turner, S., Chowdhury, A., Vernon, C. R., Hu, H., Zhuang, Y., Hejazi, M., et al.: Enhancing the representation of water management in global hydrological models, Geoscientific Model Development Discussions, pp. 1–41, 2023.

Ambec, S. and Doucet, J. A.: Decentralizing hydro power production, Canadian Journal of Economics/Revue canadienne d'économique, 36, 587–607, 2003.

Birman, C., Karbou, F., Mahfouf, J.-F., Lafaysse, M., Durand, Y., Giraud, G., Mérindol, L., and Hermozo, L.: Precipitation analysis over the French Alps using a variational approach and study of potential added value of ground-based radar observations, Journal of Hydrometeorology, 18, 1425–1451, 2017.

CFBR: Les barrages en France, https://www.barrages-cfbr.eu/-En-France-, 2021.

Chowdhury, A. K., Dang, T. D., Nguyen, H. T., Koh, R., and Galelli, S.: The Greater Mekong's climate-water-energy nexus: How ENSO-triggered regional droughts affect power supply and CO2 emissions, Earth's Future, 9, e2020EF001 814, 2021.

Dang, T. D., Chowdhury, A. K., and Galelli, S.: On the representation of water reservoir storage and operations in large-scale hydrological models: implications on model parameterization and climate change impact assessments, Hydrology and Earth System Sciences, 24, 397–416, 2020.

European Commission and Joint Research Centre (JRC): JRC Hydro-power database, http://data.europa.eu/89h/52b00441-d3e0-44e0-8281-fda86a63546d, 2019.

Fekete, B. M., Wisser, D., Kroeze, C., Mayorga, E., Bouwman, L., Wollheim, W. M., and Vörösmarty, C.: Millennium ecosystem assessment scenario drivers (1970–2050): climate and hydrological alterations, Global Biogeochemical Cycles, 24, 2010.

François, B.: Gestion optimale d'un réservoir hydraulique multiusages et changement climatique. Modèles, projections et incertitudes: Application à la réserve de Serre-Ponçon, Ph.D. thesis, Université de Grenoble, 2013.

Fumière, Q., Déqué, M., Nuissier, O., Somot, S., Alias, A., Caillaud, C., Laurantin, O., and Seity, Y.: Extreme rainfall in Mediterranean France during the fall: added value of the CNRM-AROME Convection-Permitting Regional Climate Model, Climate Dynamics, 55, 77–91, 2020.

Gottardi, F., Obled, C., Gailhard, J., and Paquet, E.: Régionalisation des précipitations sur les massifs montagneux français à l'aide de régressions locales et par types de temps, Climatologie, 5, 7–25, 2008.

Habets, F., Etchevers, P., Golaz, C., Leblois, E., Ledoux, E., Martin, E., Noilhan, J., and Ottlé, C.: Simulation of the water budget and the river flows of the Rhone basin, Journal of Geophysical Research: Atmospheres, 104, 31 145–31 172, 1999.

Haddeland, I., Skaugen, T., and Lettenmaier, D. P.: Anthropogenic impacts on continental surface water fluxes, Geophysical Research Letters, 33, 2006.

Hanasaki, N., Kanae, S., and Oki, T.: A reservoir operation scheme for global river routing models, Journal of Hydrology, 327, 22–41, 2006.

Krinner, G., Viovy, N., de Noblet-Ducoudré, N., Ogée, J., Polcher, J., Friedlingstein, P., Ciais, P., Sitch, S., and Prentice, I. C.: A dynamic global vegetation model for studies of the coupled atmosphere-biosphere system, Global Biogeochemical Cycles, 19, 2005.

Lehner, B., Czisch, G., and Vassolo, S.: The impact of global change on the hydropower potential of Europe: a model-based analysis, Energy Policy, 33, 839–855, 2005.

Lehner, B., Liermann, C. R., Revenga, C., Vörösmarty, C., Fekete, B., Crouzet, P., Döll, P., Endejan, M., Frenken, K., Magome, J., et al.: High-resolution mapping of the world's reservoirs and dams for sustainable river-flow management, Frontiers in Ecology and the Environment, 9, 494–502, 2011.

Lund, J. R. and Guzman, J.: Derived operating rules for reservoirs in series or in parallel, Journal of water resources planning and management, 125, 143–153, 1999.

Magand, C., Ducharne, A., Tilmant, F., Le Moine, N., Sauquet, E., Mathevet, T., Vidal, J.-P., and Perrin, C.: Hybridation de réanalyses météorologiques de surface pour les zones de montagne: exemple du produit DuO sur le bassin de la Durance, La Houille Blanche, pp. 77–85, 2018.

Nazemi, A. and Wheater, H. S.: On inclusion of water resource management in Earth system models, Part 1: Problem definition and representation of water demand, Hydrology and Earth System Sciences, 19, 33–61, https://doi.org/10.5194/hess-19-33-2015, 2015a.

Nazemi, A. and Wheater, H. S.: On inclusion of water resource management in Earth system models, Part 2: Representation of water supply and allocation and opportunities for improved modeling, Hydrology and Earth System Sciences, 19, 63–90, https://doi.org/10.5194/hess-19-63-2015, 2015b.

Neverre, N.: Rareté de l'eau et relations interbassins en Méditerranée sous changements globaux. Développement et application d'un modèle hydroéconomique à large échelle, Ph.D. thesis, Université Paris-Saclay (ComUE), 2015.

Nguyen-Quang, T., Polcher, J., Ducharne, A., Arsouze, T., Zhou, X., Schneider, A., and Fita, L.: ORCHIDEE-ROUTING: revising the river routing scheme using a high-resolution hydrological database, Geoscientific Model Development, 11, 4965–4985, 2018.

ODRÉ: Registre 2015 des installations de production raccordées au réseau de transport d'électricité, https://www.data.gouv.fr/fr/datasets/registre-2015-des-installations-de-production-raccordees-au-reseau-de-transport-delectricite/, 2015.

ODRÉ: Registre 2016 des installations de production raccordées au réseau de transport d'électricité, https://www.data.gouv.fr/fr/datasets/registre-2016-des-installations-de-production-raccordees-au-reseau-de-transport-delectricite/, 2016.

ODRÉ: Registre national des installations de production et de stockage d'électricité (au 31 décembre 2018), https://www.data.gouv.fr/fr/datasets/registre-national-des-installations-de-production-et-de-stockage-delectricite-au-31-decembre-2018/, 2018.

Oikonomou, K., Tarroja, B., Kern, J., and Voisin, N.: Core process representation in power system operational models: Gaps, challenges, and opportunities for multisector dynamics research, Energy, 238, 122 049, 2022.

Polcher, J., Schrapffer, A., Dupont, E., Rinchiuso, L., Zhou, X., Boucher, O., Mouche, E., Ottlé, C., and Servonnat, J.: Hydrological modelling on atmospheric grids; using graphs of sub-grid elements to transport energy and water, EGUsphere, pp. 1–34, 2023.

Quintana-Segui, P., Le Moigne, P., Durand, Y., Martin, E., Habets, F., Baillon, M., Canellas, C., Franchisteguy, L., and Morel, S.: Analysis of near-surface atmospheric variables: Validation of the SAFRAN analysis over France, Journal of applied meteorology and climatology, 47, 92–107, 2008.

Ralston Fonseca, F., Craig, M., Jaramillo, P., Bergés, M., Severnini, E., Loew, A., Zhai, H., Cheng, Y., Nijssen, B., Voisin, N., et al.: Effects of climate change on capacity expansion decisions of an electricity generation fleet in the Southeast US, Environmental Science & Technology, 55, 2522–2531, 2021.

Reynolds, C., Jackson, T., and Rawls, W.: Estimating soil water-holding capacities by linking the Food and Agriculture Organization soil map of the world with global pedon databases and continuous pedotransfer functions, Water Resources Research, 36, 3653–3662, 2000.

RTE: Generated power aggregated by sector, https://www.services-rte.com/en/download-data-published-by-rte.html?category=generation&type=actual_generations_per_production_type, a.

RTE: Hydraulic stock, https://www.services-rte.com/en/download-data-published-by-rte.html?category=generation&type=water_reserves, b.

RTE, Syndicat des Energies Renouvelables, ENEDIS, ADEeF, and Agence ORE: Panorama de l'électricité renouvelable en 2016, https://www.actu-environnement.com/media/pdf/news-28448-panorama-electricite-renouvelable-pour-annee-2016.pdf, 2016.

RTE, Syndicat des Energies Renouvelables, ENEDIS, ADEeF, and Agence ORE: Panorama de l'électricité renouvelable en 2018, /https://assets.rte-france.com/prod/public/2020-06/Panorama%20de%20l%27%C3%A9lectricit%C3%A9%20renouvelable%20au%2031%20decembre%202018_compressed.pdf, 2018.

Schapi: HydroPortail, https://hydro.eaufrance.fr/, 2022.

Siala, K., Chowdhury, A. K., Dang, T. D., and Galelli, S.: Solar energy and regional coordination as a feasible alternative to large hydropower in Southeast Asia, Nature Communications, 12, 4159, 2021.

Sterl, S., Vanderkelen, I., Chawanda, C. J., Russo, D., Brecha, R. J., Van Griensven, A., van Lipzig, N. P., and Thiery, W.: Smart renewable electricity portfolios in West Africa, Nature sustainability, 3, 710–719, 2020.

Stoft, S.: Power system economics: designing markets for electricity, vol. 468, IEEE press Piscataway, 2002.

Tabary, P., Dupuy, P., L'Henaff', G., Gueguen, C., Moulin, L., and Laurentin, O.: A 10-year (1997—2006) reanalysis of Quantitative Precipitation Estimation over France: methodology and first results, IAHS-AISH publication, pp. 255–260, 2012.

Turner, S. W. and Voisin, N.: Simulation of hydropower at subcontinental to global scales: a state-of-the-art review, Environmental Research Letters, 2022.

Turner, S. W., Ng, J. Y., and Galelli, S.: Examining global electricity supply vulnerability to climate change using a high-fidelity hydropower dam model, Science of the Total Environment, 590, 663–675, 2017.

Van Vliet, M. T., Wiberg, D., Leduc, S., and Riahi, K.: Power-generation system vulnerability and adaptation to changes in climate and water resources, Nature Climate Change, 6, 375–380, 2016.

Voisin, N., Dyreson, A., Fu, T., O'Connell, M., Turner, S. W., Zhou, T., and Macknick, J.: Impact of climate change on water availability and its propagation through the Western US power grid, Applied Energy, 276, 115 467, 2020.

Wagner, T., Themeßl, M., Schüppel, A., Gobiet, A., Stigler, H., and Birk, S.: Impacts of climate change on stream flow and hydro power generation in the Alpine region, Environmental Earth Sciences, 76, 1–22, 2017.

Wood, A. J., Wollenberg, B. F., and Sheblé, G. B.: Power generation, operation, and control, John Wiley & Sons, 2013.

Yamazaki, D. I., Jeison, S., Paul, D. B., George, H. A., and Tamlin, M. P.: MERIT Hydro: A high-resolution global hydrography map based on latest topography datasets, Water Resources Research, 55, 5053–5073, 2019.

Zhou, T., Voisin, N., and Fu, T.: Non-stationary hydropower generation projections constrained by environmental and electricity grid operations over the western United States, Environmental Research Letters, 13, 074 035, 2018.

Zhou, X., Polcher, J., and Dumas, P.: Representing human water management in a land surface model using a supply/demand approach, Water Resources Research, 57, e2020WR028 133, 2021.